Structural Engineering and Mechanics, *Vol. 70, No. 3 (2019) 351-365*
DOI: https://doi.org/10.12989/sem.2019.70.3.351

Free vibration of Cooper-Naghdi micro saturated porous sandwich cylindrical shells with reinforced CNT face sheets under magneto-hydro-thermo-mechanical loadings

Raziye Yazdani, Mehdi Mohammadimehr* and Borhan Rousta Navi

Department of Solid Mechanics, Faculty of Mechanical Engineering, University of Kashan, P.O. Box:87317-53153, Kashan, Iran

(Received May 23, 2018, Revised February 21, 2019, Accepted February 24, 2019)

Abstract. In this paper, free vibration of Cooper-Naghdi micro sandwich cylindrical shell with saturated porous core and reinforced carbon nanotube (CNT) piezoelectric composite face sheets is investigated by using first order shear deformation theory (FSDT) and modified couple stress theory (MCST). The sandwich shell is subjected to magneto-thermo-mechanical loadings with temperature dependent material properties. Energy method and Hamilton's principle are used for deriving of the motion equations. The equations are solved by Navier's method. The results are compared with the obtained results by the other literatures. The effects of various parameters such as saturated porous distribution, geometry parameters, volume fraction and temperature change on the natural frequency of the micro-sandwich cylindrical shell are addressed. The obtained results reveal that the natural frequency of the micro sandwich cylindrical shell increases with increasing of the radius to thickness ratio, Skempton coefficient, the porosity of the core, and decreasing of the length to radius ratio and temperature change.

Keywords: Cooper-Naghdi micro sandwich cylindrical shell; carbon nanotube reinforced piezoelectric composite; first order shear deformation theory; modified couple stress theory; saturated porous distribution; free vibration

1. Introduction

In recent years, cylindrical shells are the major parts in various industries that are employed in gas turbines, rotary kilns, aircrafts, spacecraft, tankers, pipelines and so on. For proper design, strength to weight ratio of shell should be as high as possible for material consumption and optimal cost reductions. Combinations of material in the nano-scale can be developed for new engineering application such as photocatalytic oxidation reactions (Zhang and Park (2017a)), visible-light driven trichloroethylene degradation (Zhang and Park (2018a)), light-driven hydrogen peroxide production (Zhang and Park (2018b)), and efficient photoreduction of aqueous Cr (Zhang and Park (2019). Hence, sandwich structures have been used to achieve this goal. A sandwich structure consists of a combination of light and thick core and two thin composite face sheets. One of the novelty materials that are used in the sandwich structure is porous materials. The main concerns about sandwich structures are the possibility of cracks and bending at the joint between face sheets and core due to the tension concentration of the stiffness difference. For solving it, reinforced fiber composite materials are used. Carbon nanotubes (CNTs) and boron nitride nanotubes (BNNTs) can be used as the reinforcement materials in various structures including sandwich beam, plate and shells. Special properties of CNTs, such as the high Yang's modulus and good tensile strength on one side, and the nature's of carbon (light weighted, very stable and simple material for processes rather than metals) can be practically useful for these structures. The porous composite sandwich shell is developed for electrochemical capacitor (Jiyoung *et al*. (2018)), super capacitor (Guijun *et al*. (2018), Zhang *et al*. (2018)), fuel cell (Chen *et al*. (2018)), high-performance supercapacitor (Zhang and Park (2017c)) and high temperature applications (Gui *et al*. (2018)).

Couple stress based strain gradient theory for elasticity is developed by Yang *et al*. (2002). Their symmetric couple stress relations (the displacement gradient (strain tensor) and the rotation gradient (symmetric curvature tensor) included the symmetric curvature tensor with properly conjugated high order strain measures for total strain energy of the system. They used modification relation for the torsion of a cylindrical bar and the pure bending of a flat plate of infinite width. In the other study, some researchers used from size dependent theory such as nonlocal elasticity theory (Murmu *et al*. (2012), Mohammadimehr and Rahmati (2013), Ke *et al*. (2015)), modified couple stress theory (MCST) (Tsiatas (2009), Shaat and Mohamed (2014), Shaat *et al*. (2014), Li and Pan (2015), Dehrouyeh Semnani *et al*. (2015), Lei *et al*. (2015)), modified strain gradient theory (Mohammadimehr *et al*. (2016a,c)).

Ansari *et al*. (2011) extended first order shear deformation theory (FSDT) for functionally graded materials nanoshell vibration. They indicated that the amount of the natural frequency decreases with increasing of the length to thickness ratio of micro beams for all the small-scale parameter values. Akbari Alashti and Khorsand (2012) examined three-dimensional elastic analysis for FG

*Corresponding author, Associate Professor
E-mail: mmohammadimehr@kashanu.ac.ir

http://www.techno-press.com/journals/sem&subpage=7
ISSN: 1225-4568 (Print), 1598-6217 (Online)

cylindrical shells with piezoelectric layers under dynamic and thermal loads. They illustrated that the distribution ratio of metal to ceramics and electrical loading has a more prominent role in the stress distribution than other parameters. Jabbari *et al*. (2013) analyzed the buckling of the porous circular plate with piezoelectric layers under the uniform compressive wave. They showed that in plates with great porosity, increasing the piezoelectric layers are more effective than the increase in the thickness of the porous in flexibility of plate.

The vibrational and damping behaviors of sandwich shells using Rayleigh and finite element methods are investigated by Yang *et al*. (2014). They found that there is an appropriate approximation between theoretical and experimental results. Ghorbanpour Arani and Amir (2013) completed electro-thermal vibration analysis of the double-walled boron nitride nanotubes (DWBNNTs) using differential quadrature method (DQM). They depicted that increasing of temperature and aspect ratio, reduces the natural frequency but increasing of Winkler modulus increases the natural frequency. Zeighampour and Tadi Beni (2014) modeled free vibration of the thin cylindrical shell. They concluded that the rigidity of the nanoshell in the modified strain gradient theory is greater than that in classical models which leads to the increase in natural frequencies. Bahadori and Najafizadeh (2015) investigated the free vibration of two dimensional functionally graded cylindrical thick shell surrounded by Winkler–Pasternak elastic foundation based on FSDT theory. They showed that the natural frequencies in this case are more than cases in which properties are changed merely in one direction. Tadi Beni *et al*. (2015) studied the small-length scale parameter in cylindrical nano shells using MCST. They proved that increasing of the small length scale increases the natural frequencies of the system. Mohammadimehr and Alimirzaei (2016) presented nonlinear static and vibration analysis of Euler-Bernoulli composite beam model reinforced by FG-SWCNT with initial geometrical imperfection using FEM.

Shaat (2015) found effects of grain size and microstructure rigid rotations on the bending behavior of nanocrystalline material beams. They showed that bending rigidity changes for the grain size effects and microstructure rotations based on MCST. In the other work, Shaat and Abdelkefi (2015) also studied modeling the material structure and couple stress effects of nanocrystalline silicon beams for pull-in and bio-mass sensing applications. They used the MCST and size-dependent micromechanical model including the interface and the grain size effects to estimate the beam's size effect and the heterogeneity nature of the material structure, respectively. Physical and mathematical representations of couple stress effects on micro/nanosolids are presented by Shaat (2015). He used two higher-order material constants in classic couple stress theory. The modified couple stress theory includes rotational effect of the applied force inside its conventional effects. They concluded that the skew-symmetric rotation gradient tensor is the measure used to capture the couple stress effects.

Pourasghar and Kamarian (2016) obtained thermoelastic response of CNT reinforced cylindrical panel resting on elastic foundation using elasticity theory with temperature-dependent materials. Kamarian and Shakeri (2016) performed the natural frequency analysis of composite skew plates with embedded shape memory alloys in thermal environment. They showed that with an increase in the temperature, the initial natural frequency of the plate without sequential multiplex amplification (SMA) continuously decreases to zero, but for the plate with a booster, firstly the natural frequency decreases, then reach to the maximum, and finally reaches to zero.

Ghorbanpour Arani *et al*. (2016) investigated free vibration of sandwich composite micro-plate under electric and magnetic fields. They used DQM to indicate the important effects of material length scale parameter, aspect ratios, different fiber angles, electro-magneto-mechanical loadings on sandwich composite microplate frequency. Razavi *et al*. (2016) performed free vibration analysis of functionally graded piezoelectric cylindrical nanoshell based on consistent couple stress theory using Navier's and Galerkin methods. They proved that geometric parameters play a significant role on the natural frequency values with the size-dependent piezoelectric theory. Dey and Ramachandra (2016) developed non-linear transverse dynamic response of laminated composite simply supported circular cylindrical shell under periodic radial point and static axial partial loadings. They showed that the amplitude of the frequency is influenced by the total load, not the manner in which it is applied. Kheibari and Tadi Beni (2016) investigated free vibration of piezoelectric nanotubes by using consistent couple stress theory and based on Love's cylindrical thin-shell model. They indicated that by increasing the size parameter, the natural frequency increases. Vibrations behavior of a temperature-dependent functionally graded rectangular plates with simply-supported boundary condition subjected to thermal load is performed by Dong and Li (2016). They revealed that the natural frequency decreases with presence of the thermal load. The high-order free vibration analysis of two type sandwich beams including CNTs reinforced nanocomposite face sheets and different core is studied by Mohammadimehr and shahedi (2016).

The Vibration analysis of CNT reinforced functionally graded composite cylindrical shell in thermal environments is carried out by Song *et al*. (2016). They investigated the CNTs distribution, CNTs volume fractions and thermal effects on the natural frequency. Mohammadimehr & Mostafavifar (2016) studied the free vibration of temperature-dependent sandwich plate with FG-CNTs reinforced nanocomposite face sheets under magnetic field. They proved that although dimensionless natural frequency increases with rising the aspect ratio and magnetic field, it decreases by increasing the temperature.

Mohammadimehr *et al*. (2016b) performed the vibrations of composite plate reinforced with different FG-SWCNT under electric-magnetic field using FSDT. They showed that with increasing the volume fraction of SWCNT, the natural frequency of the system increases. Also, the presence of the elastic foundation raises the natural frequency. Free vibration of double-bonded micro composite sandwich cylindrical shells conveying fluid flow is investigated by Mohammadimehr and Mehrabi (2017). Their study showed that increasing of the magnetic intensity and volume fraction leads to increase the dimensionless

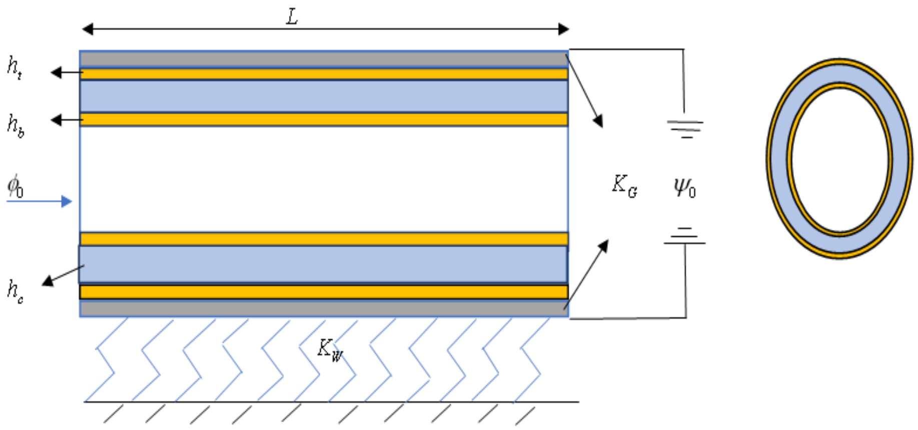

Fig. 1 Schematic view of circular micro sandwich cylindrical shell

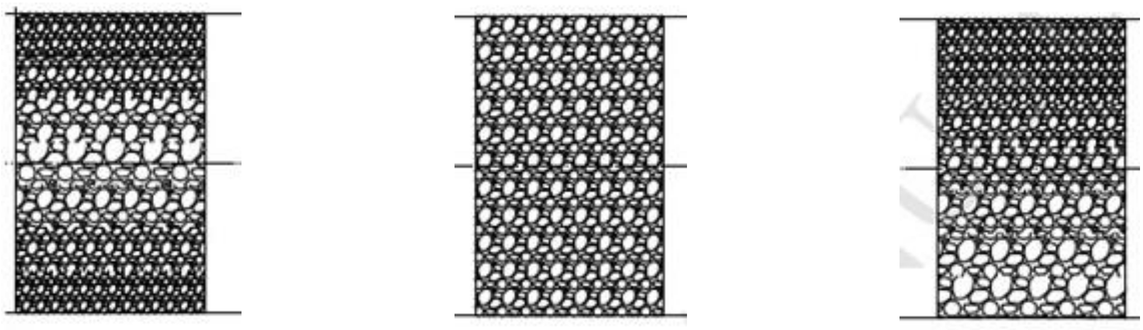

c- b- a-

Fig. 2 Porosity for core of the micro sandwich cylindrical shell a- porous-nonlinear nonsymmetric b- porous-monotonous c- porous-nonlinear symmetric (Jabbari *et al*. (2013))

natural frequency of the micro shells. Static stress analysis of carbon nanotube reinforced composite (CNTRC) cylinder under non-axisymmetric thermo-mechanical loads and uniform electromagnetic fields is developed by Ghorbanpour Arani et. al. (2015). They concluded that CNTs and its orientation angle have important effects on the mechanical behavior of the CNTRC cylinder composite. Dynamic responses of embedded double-layered graphene sheets under longitudinal magnetic field with arbitrary boundary conditions are performed by Jalaei and Ghorbanpour Arani (2018). They showed that magnetic field effect on deflection is more considerable for higher nonlocal parameter. Shen et. al. (2018) analyzed nonlinear vibration of functionally graded graphene-reinforced composite laminated cylindrical panels resting on elastic foundations in thermal environments.

Thermal conductivity and thermo-physical properties of nanodiamond-attached exfoliated hexagonal boron nitride/epoxy nanocomposites presented by Zhang *et al.* (2017a, b).

In this paper, the free vibration responses of Cooper-Naghdi micro sandwich cylindrical shell with saturated porous core and reinforced carbon nanotube piezoelectric composite face sheets under magneto-hydro-thermo-mechanical loadings is investigated. Modified couple stress theory and Cooper-Naghdi shell theory are used for this research. Material properties are function of temperature change. After obtaining the governing equations using Hamilton's principle, they are solved by Navier's method, then, the effects of different factors on the natural frequency for the micro sandwich shell are presented.

2. Geometry and simulation

Fig. 1 illustrates the schematic of micro sandwich cylindrical shell with saturated porous core and reinforced carbon nanotube piezoelectric composite face sheets under magneto-hydro-thermo-mechanical loadings. Length, thickness and inner radius of the micro sandwich cylindrical shell are L, h and R respectively. h_c is the thickness of core, and, h_b and h_t are for lower and upper face sheets, respectively. The micro sandwich cylindrical shell with temperature dependent material properties is embedded by Winkler-Pasternak foundation with K_W and K_G. The micro sandwich cylindrical shell is subjected to applied voltage ψ_0 and magnetic field ϕ_0.

Fig. 2 shows three distribution types of porous material (porous nonlinear-nonsymetric, porous-monotonous and porous-nonlinear-symmetric) along thickness of the micro sandwich cylindrical shell. The initial shear modulus, Poisson's ratio and density are $G_0 = 24GPa$, $\nu_0 = 0.3$ and ρ_0

= 2700kg/ m^3 (Jabbari *et al*. (2013)).

According to variation of porous distribution types along thickness, the following relations can be written (Jabbari *et al*. (2013)):

For porous nonlinear-nonsymetric distribution

$$\begin{aligned} G(z) &= G_0(1-e_1\cos((\frac{\pi}{2h})(z+\frac{h}{2}))) \\ E(z) &= E_0(1-e_1\cos((\frac{\pi}{2h})(z+\frac{h}{2}))) \\ \rho(z) &= \rho_0(1-e_1\cos((\frac{\pi}{2h})(z+\frac{h}{2}))) \end{aligned} \tag{a-1}$$

For porous-monotonous distribution (Jabbari *et al*. (2013))

$$\begin{aligned} G(z) &= G_0(1-e_1\cos(\frac{\pi z}{h})) \\ E(z) &= E_0(1-e_1\cos(\frac{\pi z}{h})) \\ \rho(z) &= \rho_0(1-e_1\cos(\frac{\pi z}{h})) \end{aligned} \tag{b-1}$$

For porous-nonlinear-symmetric distribution (Jabbari *et al*. (2013))

$$\begin{aligned} G(z) &= G_0(1-e_1) \\ E(z) &= E_0(1-e_1) \\ \rho(z) &= \rho_0(1-e_1) \end{aligned} \tag{c-1}$$

Extended mixture approach is used for effective material properties of upper and lower face sheets as follows (Ghorbanpour Arani *et al*. (2016, 2012), Mohammadimehr *et al*. (2018a, b))

$$\begin{aligned} E_{11} &= \eta_1 V_{SWCNT} E_{11}^{SWCNT} + V_m E_m \\ \frac{\eta_2}{E_{22}} &= \frac{V_{SWCNT}}{E_{22}^{SWCNT}} + \frac{V_m}{E_m} \\ \frac{\eta_3}{G_{12}} &= \frac{V_{SWCNT}}{G_{12}^{SWCNT}} + \frac{V_m}{G_m} \end{aligned} \tag{2}$$

where, η_i (i = 1,2,3) are efficiency coefficients of SWCNTs. These coefficients are listed in Table 1. E_{11}, E_{22} and G_{12} are the Young's modulii and the shear modulus of the SWCNT, and V_{SWCNT} and $\underline{V}m$ are the volume fraction of the WCNT and the matrix, respectively. The material properties of SWCNTs for different temperatures are listed in Table 2. Various distributions of SWCNT are defined as (Ghorbanpour Arani *et al*. (2016), Mohammadimehr *et al*. (2018a))

$$V_{SWCNT}(z) = \begin{cases} V^*_{SWCNT} & (UD-SWCNT) \\ (1+\frac{2z}{h})V^*_{SWCNT} & (FG-V-SWCNT) \\ 2(1-\frac{|2z|}{h})V^*_{SWCNT} & (FG-O-SWCNT) \\ 2\frac{|2z|}{h}V^*_{SWCNT} & (FG-X-SWCNT) \end{cases} \tag{3}$$

where

$$\overset{*}{V}_{SWCNT} = \frac{w_{SWCNT}}{w_{SWCNT} + \left(\frac{\rho_{SWCNT}}{\rho_m}\right)(1-w_{SWCNT})} \tag{4}$$

where, w_{SWCNT} is the mass fraction of the nanotubes. ρ_{SWCNT} and ρ_m are densities of SWCNTs and the matrix, respectively.

Density, Poison's ratios, thermal and hydro properties of face sheets are written as (Ghorbanpour Arani *et al*. (2016), Mohammadimehr *et al*. (2018a, b))

$$\begin{aligned} \rho &= \rho_{SWCNT}V_{SWCNT} + \rho_m V_m \\ \nu_{12} &= \nu_{12}^{SWCNT}V_{SWCNT} + \nu_m V_m \\ \alpha_{11} &= \alpha_{11}^{SWCNT}V_{SWCNT} + \alpha_m V_m \\ \alpha_{22} &= (1+\nu_{12}^{SWCNT})\alpha_{22}^{SWCNT}V_{SWCNT} + (1+\nu_m)\alpha_m V_m - \nu_{12}\alpha_{11} \\ \beta_{11} &= \beta_{11}^{SWCNT}V_{SWCNT} + \beta_m V_m \\ \beta_{22} &= (1+\nu_{12}^{SWCNT})\beta_{22}^{SWCNT}V_{SWCNT} + (1+\nu_m)\beta_m V_m - \nu_{12}\beta_{11} \end{aligned} \tag{5}$$

The face sheets are reinforced by SWCNTs. The volume fractions of SWCNTs for the top and the bottom of face sheets are as (Ghorbanpour Arani *et al*. (2016))

$$\begin{aligned} V_{CNTt} &= 2\left(\frac{t_1 - z}{t_1 - t_0}\right)\overset{*}{V}_{CNT} \\ V_{CNTb} &= 2\left(\frac{z - t_2}{t_3 - t_2}\right)\overset{*}{V}_{CNT} \end{aligned} \tag{6}$$

Stiffness, piezoelectric and magnetic coefficients for face sheets can be stated as (Ghorbanpour Arani *et al*. (2016), Mohammadimehr *et al*. (2016a)).

$$\begin{aligned} & Q_{11}(z) = \frac{E_{11}(z)}{1-\upsilon_{12}(z)\upsilon_{21}(z)}, \quad e_{24} = V_{SWNT}e_{24}^{SWNT} + (1-V_{SWNT})e_{24}^{m} \\ & Q_{22}(z) = \frac{E_{22}(z)}{1-\upsilon_{12}(z)\upsilon_{21}(z)}, \quad e_{32} = V_{SWNT}e_{32}^{SWNT} + (1-V_{SWNT})e_{32}^{m} \\ & Q_{12}(z) = \frac{\upsilon_{21}(z)E_{11}(z)}{1-\upsilon_{12}(z)\upsilon_{21}(z)}, \\ & e_{31} = q_{11}((\frac{(1-V_{SWNT})e_{31}^{SWNT}}{q_{11}^{SWNT}}) + (\frac{V_{SWNT}e_{31}^{m}}{q_{11}^{m}})) \\ & Q_{44}(z) = \frac{E_{22}(z)}{2(1+\upsilon_{23}(z))}, \quad e_{15} = \frac{e_{15}^{m}e_{15}^{SWNT}}{V_{SWNT}e_{15}^{m} + (1-V_{SWNT})e_{15}^{SWNT}} \\ & Q_{55}(z) = Q_{66}(z) = G_{12}(z), \\ & \eta_{11} = (1-V_{SWNT})\eta_{11}^{m} + V_{SWNT}\eta_{11}^{SWNT} \\ & \eta_{22} = (1-V_{SWNT})\eta_{22}^{m} + V_{SWNT}\eta_{22}^{SWNT}, \\ & \eta_{33} = (1-V_{SWNT})\eta_{33}^{m} + V_{SWNT}\eta_{33}^{SWNT} \end{aligned} \tag{7}$$

Displacement fields of the micro sandwich moderately cylindrical shell based on Cooper-Naghdi theory are given by (Cooper and Naghdi (1957), Bahadori and Najafizadeh (2015)).

Table 1 Efficiency coefficients of SWCNTs (Ghorbanpour Arani *et al*. (2016))

V^*_{CNT}	η_1	η_2	η_3
0.11	0.149	0.934	0.934
0.14	0.150	0.941	0.941
0.17	0.149	1.381	1.381

Table 2 Temperature dependent material properties for (10, 10) SWCNT (R=0.68nm, L=9.26nm, h=0.067 nm, ρ = 1400kg/m ^{3}, ν_{12} = 0.175) (Farajpour *et al*. (2016)).

Temperature (K)	E_{11}^{CNT} (TPa)	E_{22}^{CNT} (TPa)	G_{12}^{CNT} (TPa)	α_{11}^{CNT} $(1/GPa.K)$	α_{12}^{CNT} $(1/GPa.K)$
300	5.6466	7.08	1.9445	3.4584	5.1682
500	5.5308	6.9348	1.9643	4.5361	5.0189
700	5.4744	6.8641	1.9644	4.6677	4.8943

$$\begin{aligned} U_x(x,\theta,z,t) &= u(x,\theta,t) + z\,\beta_x(x,\theta,t) \\ U_\theta(x,\theta,z,t) &= v(x,\theta,t) + z\,\beta_\theta(x,\theta,t) \\ U_z(x,\theta,z,t) &= w(x,\theta,t) \end{aligned} \tag{8}$$

where, $u(x, \theta, t)$, $v(x, \theta, t)$, $w(x, \theta, t)$, $\beta_x(x, \theta, t)$ and $\beta_\theta(x, \theta, t)$ are middle surface displacements and rotations in the longitudes, peripheral and thickness direction of the micro sandwich moderately cylindrical shell, respectively.

Strain–displacement relations for each of face sheet and core can be expressed as (Tadi Beni *et al*. (2015)):

$$\begin{aligned} \varepsilon_{xx} &= \frac{\partial U_x}{\partial x} = \frac{\partial u}{\partial x} + z\,\frac{\partial \beta_x}{\partial x} \\ \varepsilon_{\theta\theta} &= \frac{U_z}{R} + \frac{1}{R}\frac{\partial U_\theta}{\partial \theta} = \frac{1}{R}(w + \frac{\partial v}{\partial \theta} + z\,\frac{\partial \beta_\theta}{\partial \theta}) \\ \varepsilon_{z\theta} &= \frac{1}{2}(\frac{1}{R}\frac{\partial U_z}{\partial \theta} + \frac{\partial U_\theta}{\partial z} - \frac{v}{R}) = \frac{1}{2}(\frac{1}{R}\frac{\partial w}{\partial \theta} + \beta_\theta - \frac{v}{R}) \\ \varepsilon_{xz} &= \frac{1}{2}(\frac{\partial U_z}{\partial x} + \frac{\partial U_x}{\partial z}) = \frac{1}{2}(\frac{\partial w}{\partial x} + \beta_x) \\ \varepsilon_{\theta x} &= \frac{1}{2}(\frac{1}{R}\frac{\partial U_x}{\partial \theta} + \frac{\partial U_\theta}{\partial x}) = \frac{1}{2}(\frac{1}{R}(\frac{\partial u}{\partial \theta} + z\,\frac{\partial \beta_x}{\partial \theta}) + \frac{\partial v}{\partial x} + z\,\frac{\partial \beta_\theta}{\partial x} \end{aligned} \tag{9}$$

Hamilton's principle can be stated as follows:

$$\int_0^t (\delta T - \delta U - \delta W)dt = 0 \tag{10}$$

where δU. δW and δT are the variations of strain energy, work done by external force and kinetic energy, respectively.

The variation of strain energy for three layers of the micro sandwich moderately cylindrical shell based on modified couple stress theory can be written as follows:

$$\begin{aligned} \delta U &= \frac{1}{2}\int_{-\frac{h_c}{2}-h_b}^{-\frac{h_c}{2}} (\sigma_{ij}\delta\varepsilon_{ij} + m_{ij}\delta\chi_{ij} - D_i\delta E_i - B_i\delta H_i)dV \\ &+ \frac{1}{2}\int_{-\frac{h_c}{2}}^{-\frac{h_c}{2}} (\sigma_{ij}\delta\varepsilon_{ij} + m_{ij}\delta\chi_{ij})dV \\ &+ \frac{1}{2}\int_{\frac{h_c}{2}}^{\frac{h_c}{2}+h_t} (\sigma_{ij}\delta\varepsilon_{ij} + m_{ij}\delta\chi_{ij} - D_i\delta E_i - B_i\delta H_i)dV \end{aligned} \tag{11}$$

where the stress tensor σ_{ij}, symmetric stress tensor m_{ij} and symmetric rotation gradient tensor are defined as (Tadi Beni *et al*. (2015)):

$$\begin{Bmatrix} \sigma_{xx} \\ \sigma_{\theta\theta} \\ \sigma_{z\theta} \\ \sigma_{zx} \\ \sigma_{x\theta} \end{Bmatrix} = \begin{bmatrix} Q_{11} & Q_{12} & 0 & 0 & 0 \\ Q_{12} & Q_{22} & 0 & 0 & 0 \\ 0 & 0 & k_s Q_{44} & 0 & 0 \\ 0 & 0 & 0 & k_s Q_{55} & 0 \\ 0 & 0 & 0 & 0 & Q_{66} \end{bmatrix} \begin{Bmatrix} \varepsilon_{xx} - \alpha_{11}\Delta T \\ \varepsilon_{\theta\theta} - \alpha_{22}\Delta T \\ \gamma_{z\theta} \\ \gamma_{zx} \\ \gamma_{x\theta} \end{Bmatrix}$$

$$- \begin{bmatrix} 0 & 0 & e_{31} \\ 0 & 0 & e_{32} \\ 0 & e_{24} & 0 \\ e_{15} & 0 & 0 \\ 0 & 0 & 0 \end{bmatrix} \begin{Bmatrix} E_x \\ E_\theta \\ E_z \end{Bmatrix} - \begin{bmatrix} 0 & 0 & q_{31} \\ 0 & 0 & q_{32} \\ 0 & q_{24} & 0 \\ q_{15} & 0 & 0 \\ 0 & 0 & 0 \end{bmatrix} \begin{Bmatrix} H_x \\ H_\theta \\ H_z \end{Bmatrix},$$

$$\begin{aligned} m_{ij} &= 2l^2\mu\chi_{ij}, \theta_i \\ &= \frac{1}{2}curl(u), \chi_{ij} = \frac{1}{2}(\theta_{i,j} + \theta_{j,i}) \end{aligned} \tag{12}$$

$$\begin{aligned} \chi_{xx} &= \frac{1}{2}(\frac{1}{R}\frac{\partial^2 w}{\partial x\partial\theta} - \frac{1}{R}\frac{\partial v}{\partial x} - \frac{\partial\beta_\theta}{\partial x}), \\ \chi_{\theta\theta} &= \frac{1}{2R}(\frac{\partial v}{\partial x} - \frac{1}{R}\frac{\partial u}{\partial\theta} - \frac{\partial^2 w}{\partial x\partial\theta} + \frac{\partial\beta_x}{\partial\theta} + z\frac{\partial\beta_\theta}{\partial x}) \\ \chi_{zz} &= \frac{1}{2}(\frac{1}{R^2}\frac{\partial u}{\partial\theta} - \frac{1}{R}\frac{\partial\beta_x}{\partial\theta} + \frac{\partial\beta_\theta}{\partial x}), \\ \chi_{\theta x} = \chi_{x\theta} &= \frac{1}{4}(\frac{1}{R^2}(\frac{\partial^2 w}{\partial\theta^2} - \frac{\partial v}{\partial\theta}) - \frac{\partial^2 w}{\partial x^2} - \frac{1}{R}\frac{\partial\beta_\theta}{\partial\theta} + \frac{\partial\beta_x}{\partial x}) \\ \chi_{z\theta} = \chi_{\theta z} &= \frac{1}{4R}(\frac{\partial^2 v}{\partial x\partial\theta} - \frac{1}{R}\frac{\partial^2 u}{\partial\theta^2} + \frac{\partial w}{\partial x} + z\frac{\partial^2\beta_\theta}{\partial x\partial\theta} - \frac{z}{R}\frac{\partial^2\beta_x}{\partial\theta^2} - \beta_x) \\ \chi_{zx} = \chi_{xz} &= \frac{1}{4}(\frac{v}{R^2} - \frac{1}{R}\frac{\partial^2 u}{\partial\theta\partial x} + \frac{\partial^2 v}{\partial x^2} - \frac{1}{R^2}\frac{\partial w}{\partial\theta} + z\frac{\partial^2\beta_\theta}{\partial x^2} - \frac{z}{R}\frac{\partial^2\beta_x}{\partial\theta\partial x} - \frac{\beta_\theta}{R}) \end{aligned}$$

Electrical and magnetic potential functions can be expressed as

$$\begin{aligned} \psi(x,\theta,z,t) &= \frac{2\tilde{z}}{h_p}\psi_0 - \psi(x,\theta,t)\cos(\frac{\pi\tilde{z}}{h_p}) \\ \varphi(x,\theta,z,t) &= \frac{2\tilde{z}}{h_p}\varphi_0 - \varphi(x,\theta,t)\cos(\frac{\pi\tilde{z}}{h_p}) \\ \tilde{z} &= z - \frac{h_c}{2} - \frac{h_t}{2} \end{aligned} \tag{13}$$

Electric field E_i, magnetic field H_i, piezo-magnetic strain tensor B_i and dielectric displacement tensor D_i are considered as the following form (Arefi and Zenkour (2016))

$$\begin{bmatrix} E_x \\ E_\theta \\ E_z \end{bmatrix} = \begin{bmatrix} -\varphi_{,x} \\ -\dfrac{\varphi_{,\theta}}{R} \\ -\varphi_{,z} \end{bmatrix} = \begin{bmatrix} \dfrac{\partial\varphi}{\partial x}\cos(\dfrac{\pi\tilde{z}}{h_p}) \\ \dfrac{1}{R}\dfrac{\partial\varphi}{\partial\theta}\cos(\dfrac{\pi\tilde{z}}{h_p}) \\ -\dfrac{2\varphi_0}{h_p} - \dfrac{\pi}{h_p}\varphi(x,\theta,t)\sin(\dfrac{\pi\tilde{z}}{h_p}) \end{bmatrix}, \tag{14}$$

$$\begin{bmatrix} H_x \\ H_\theta \\ H_z \end{bmatrix} = \begin{bmatrix} -\psi_{,x} \\ -\dfrac{\psi_{,\theta}}{R} \\ -\psi_{,z} \end{bmatrix} = \begin{bmatrix} \dfrac{\partial \psi}{\partial x}\cos(\dfrac{\pi \tilde{z}}{h_p}) \\ \dfrac{1}{R}\dfrac{\partial \psi}{\partial \theta}\cos(\dfrac{\pi \tilde{z}}{h_p}) \\ -\dfrac{2\psi_0}{h_p} - \dfrac{\pi}{h_p}\psi(x,\theta,t)\sin(\dfrac{\pi \tilde{z}}{h_p}) \end{bmatrix}$$

$$\begin{bmatrix} D_x \\ D_\theta \\ D_z \end{bmatrix} = \begin{bmatrix} 0 & 0 & e_{31} \\ 0 & 0 & e_{32} \\ 0 & e_{24} & 0 \\ e_{15} & 0 & 0 \\ 0 & 0 & 0 \end{bmatrix}^T \begin{Bmatrix} \varepsilon_{xx} \\ \varepsilon_{\theta\theta} \\ \gamma_{z\theta} \\ \gamma_{zx} \\ \gamma_{x\theta} \end{Bmatrix} + \begin{bmatrix} k_{11} & 0 & 0 \\ 0 & k_{22} & 0 \\ 0 & 0 & k_{33} \end{bmatrix} \begin{Bmatrix} E_x \\ E_\theta \\ E_z \end{Bmatrix} + \begin{bmatrix} g_{11} & 0 & 0 \\ 0 & g_{22} & 0 \\ 0 & 0 & g_{33} \end{bmatrix} \begin{Bmatrix} H_x \\ H_\theta \\ H_z \end{Bmatrix}$$

$$\begin{bmatrix} B_x \\ B_\theta \\ B_z \end{bmatrix} = \begin{bmatrix} 0 & 0 & q_{31} \\ 0 & 0 & q_{32} \\ 0 & q_{24} & 0 \\ q_{15} & 0 & 0 \\ 0 & 0 & 0 \end{bmatrix}^T \begin{Bmatrix} \varepsilon_{xx} \\ \varepsilon_{\theta\theta} \\ \gamma_{z\theta} \\ \gamma_{zx} \\ \gamma_{x\theta} \end{Bmatrix} + \begin{bmatrix} g_{11} & 0 & 0 \\ 0 & g_{22} & 0 \\ 0 & 0 & g_{33} \end{bmatrix} \begin{Bmatrix} E_x \\ E_\theta \\ E_z \end{Bmatrix} + \begin{bmatrix} \mu_{11} & 0 & 0 \\ 0 & \mu_{22} & 0 \\ 0 & 0 & \mu_{33} \end{bmatrix} \begin{Bmatrix} H_x \\ H_\theta \\ H_z \end{Bmatrix}$$

The following relations are defined as follows (Mohammadimehr *et al*. (2018a))

$$\begin{aligned} &(N_{xx}, N_{\theta\theta}, N_{x\theta}) \\ &= \int_{-h_b - h_c/2}^{h_t + h_c/2} (\sigma_{xx}, \sigma_{\theta\theta}, \sigma_{x\theta}) dz, (M_{xx}, M_{\theta\theta}, M_{x\theta}) \\ &= \int_{-h_b - h_c/2}^{h_t + h_c/2} (\sigma_{xx}, \sigma_{\theta\theta}, \sigma_{x\theta}) z dz \\ &(Q_x, Q_\theta) \\ &= \int_{-h_b - h_c/2}^{h_t + h_c/2} (\sigma_{xz}, \sigma_{\theta z}) dz, (Y_{xx}, Y_{\theta\theta}, Y_{zz}, Y_{z\theta}, Y_{zx}, Y_{\theta x}) \\ &= \int_{-h_b - h_c/2}^{h_t + h_c/2} (m_{xx}, m_{\theta\theta}, m_{zz}, m_{z\theta}, m_{zx}, m_{\theta x}) dz \\ &(T_{xx}, T_{\theta\theta}, T_{zz}, T_{z\theta}, T_{zx}, T_{\theta x}) \\ &= \int_{-h_b - h_c/2}^{h_t + h_c/2} (m_{xx}, m_{\theta\theta}, m_{zz}, m_{z\theta}, m_{zx}, m_{\theta x}) z dz, \end{aligned} \tag{15}$$

$$\begin{bmatrix} P_x \\ P_\theta \\ P_z \end{bmatrix} = \begin{bmatrix} D_x \cos(\dfrac{\pi \tilde{z}}{h_p}) \\ \dfrac{D_\theta}{R}\cos(\dfrac{\pi \tilde{z}}{h_p}) \\ D_x(\dfrac{\pi}{h_p})\cos(\dfrac{\pi \tilde{z}}{h_p}) \end{bmatrix} dz,$$

$$\begin{bmatrix} O_x \\ O_\theta \\ O_z \end{bmatrix} = \begin{bmatrix} B_x \cos(\dfrac{\pi \tilde{z}}{h_p}) \\ \dfrac{B_\theta}{R}\cos(\dfrac{\pi \tilde{z}}{h_p}) \\ B_x(\dfrac{\pi}{h_p})\cos(\dfrac{\pi \tilde{z}}{h_p}) \end{bmatrix}$$

The variation of kinetic energy is given by:

$$\begin{aligned} &\int_\Omega \delta T = \int_{-\frac{h_c}{2}-h_b}^{\frac{h_c}{2}+h_t} \delta T + \int_{-\frac{h_c}{2}-h_b}^{\frac{h_c}{2}+h_t} \delta T + \int_{\frac{h_c}{2}}^{\frac{h_c}{2}+h_t} \delta T \\ &\delta T = \int_\Omega \rho(z)[\frac{\partial U_x}{\partial t}\delta(\frac{\partial U_x}{\partial t}) + \frac{\partial U_\theta}{\partial t}\delta(\frac{\partial U_\theta}{\partial t}) + \frac{\partial U_z}{\partial t}\delta(\frac{\partial U_z}{\partial t})]dV \\ &\delta T = \int_\Omega \rho(z)[(\frac{\partial u}{\partial t} + z\frac{\partial \beta_x}{\partial t})\delta(\frac{\partial u}{\partial t} + z\frac{\partial \beta_x}{\partial t}) + (\frac{\partial v}{\partial t} + z\frac{\partial \beta_\theta}{\partial t})\delta(\frac{\partial v}{\partial t} + z\frac{\partial \beta_\theta}{\partial t}) + (\frac{\partial w}{\partial t})\delta(\frac{\partial w}{\partial t})]dx d\theta dz \end{aligned} \tag{16}$$

Variation of kinetic energy must be extended for three layers of the micro sandwich cylindrical shell. Variation of work done by foundation forces can be written as (Mohammadimehr *et al*. (2011), (2016d))

$$\begin{aligned} &\delta W = \int_A F^{elastic} \delta w dA \\ &F^{elastic} = k_w w_0 - k_g(\frac{1}{R^2}\frac{\partial^2 w_0}{\partial \theta^2} + \frac{\partial^2 w_0}{\partial x^2}) \end{aligned} \tag{17}$$

Using Eq. (15) to Eq. (17), the governing equation of micro sandwich cylindrical shell can be obtained as follows:

$$\begin{aligned} &N_{x,x} + \frac{1}{R}N_{x\theta,\theta} - \frac{1}{2R^2}Y_{\theta,\theta} + \frac{1}{2R^2}Y_{z,\theta} + \frac{1}{2R^2}Y_{z\theta,\theta\theta} \\ &+ \frac{1}{2R}Y_{xz,x\theta} = I_{(0)}\frac{\partial^2 u}{\partial t^2} + I_{(1)}\frac{\partial^2 \beta_x}{\partial t^2} \\ &\frac{1}{R}N_{\theta,\theta} + \frac{1}{R}Q_\theta + N_{x\theta,x} - \frac{1}{2R}Y_{x,x} + \frac{1}{2R}Y_{\theta,x} - \frac{1}{2R}Y_{z\theta,x\theta} \\ &- \frac{1}{2R^2}Y_{xz} - \frac{1}{2}Y_{xz,xx} - \frac{1}{2R^2}Y_{x\theta,\theta} = I_{(0)}\frac{\partial^2 v}{\partial t^2} + I_{(1)}\frac{\partial^2 \beta_\theta}{\partial t^2} \\ &-\frac{1}{R}N_\theta + \frac{1}{R}Q_{\theta,\theta} + Q_{x,x} - \frac{1}{2R}Y_{x,x\theta} + \frac{1}{2R}Y_{\theta,x\theta} + \frac{1}{2R}Y_{z\theta,x} \\ &-\frac{1}{2R^2}Y_{xz,\theta} - \frac{1}{2R^2}Y_{x\theta,\theta\theta} + \frac{1}{2}Y_{x\theta,xx} \end{aligned} \tag{18}$$

$$+q(x,\theta)+K_w w+K_G\nabla^2 w=I_{(0)}\frac{\partial^2 w}{\partial t^2}$$

$$\begin{aligned}
&M_{x,x}-Q_x+\frac{1}{R}M_{x\theta,x}+\frac{1}{2R}Y_{\theta,\theta}\\
&-\frac{1}{2R}Y_{z,\theta}+\frac{1}{2R}Y_{z\theta}+\frac{1}{2R^2}T_{z\theta,\theta\theta}\\
&+\frac{1}{2}Y_{xz,x}+\frac{1}{2R}T_{xz,x\theta}+\frac{1}{2}Y_{x\theta,x}\\
&=I_{(1)}\frac{\partial^2 u}{\partial t^2}+I_{(2)}\frac{\partial^2\beta_x}{\partial t^2}\\
&\frac{1}{R}M_{\theta,\theta}-Q_\theta+M_{x\theta,x}-\frac{1}{2}Y_{x,x}\\
&+\frac{1}{2R}T_{\theta,x}+\frac{1}{2}Y_{z,x}-\frac{1}{2R}T_{z\theta,x\theta}\\
&+\frac{1}{2R}Y_{xz}-\frac{1}{2}T_{xz,xx}-\frac{1}{2R}Y_{x\theta,\theta}\\
&=I_{(1)}\frac{\partial^2 v}{\partial t^2}+I_{(2)}\frac{\partial^2\beta_\theta}{\partial t^2}\\
&P_{x,x}+P_{\theta,\theta}+P_z=0\\
&O_{x,x}+O_{\theta,\theta}+O_z=0
\end{aligned}$$

The coefficients of Eq. (18) are addressed in Appendix A.

Substituting Eqs. (12-15) into Eq. (18), the governing equations based on displacement are derived as:

δu :

$$\begin{aligned}
&-(D_{1,0}+A_{20})\frac{\partial^2 u}{\partial x^2}+\frac{D_{5,0}l^2}{4R^2}\frac{\partial^4 u}{\partial x^2\partial\theta^2}-\frac{D_{5,0}l^2}{R^4}\frac{\partial^2 u}{\partial\theta^2}\\
&-\frac{1}{R^2}(D_{5,0}+C_{20})\frac{\partial^2 u}{\partial\theta^2}+\frac{D_{5,0}l^2}{4R^4}\frac{\partial^4 u}{\partial\theta^4}\\
&-\frac{D_{5,0}l^2}{4R}\frac{\partial^4 v}{\partial x^3\partial\theta}+\frac{1}{R}(\frac{D_{5,0}l^2}{4R^2})\frac{\partial^2 v}{\partial x\partial\theta}\\
&-\frac{1}{R}(D_{3,0}+D_{5,0}+B_{20}+C_{20})\frac{\partial^2 v}{\partial x\partial\theta}\\
&-\frac{D_{5,0}l^2}{4R^3}\frac{\partial^4 v}{\partial x\partial\theta^3}-\frac{1}{R}(D_{3,0}+B_{20})\frac{\partial w}{\partial x}\\
&-\frac{D_{5,0}l^2}{2R^3}\frac{\partial^3 w}{\partial x\partial\theta^2}-\frac{1}{R}(\frac{D_{5,0}l^2}{4R}-\frac{D_{5,1}l^2}{2R^2})\frac{\partial^2\beta_\theta}{\partial x\partial\theta}\\
&-\frac{1}{R}(D_{3,1}+D_{5,1}+B_{21}+C_{21})\frac{\partial^2\beta_\theta}{\partial x\partial\theta}\\
&+\frac{1}{R^2}(\frac{5D_{5,0}l^2}{4R})\frac{\partial^2\beta_x}{\partial\theta^2}-\frac{1}{R^2}(C_{21}+D_{5,1})\frac{\partial^2\beta_x}{\partial\theta^2}\\
&-(D_{1,1}+A_{21})\frac{\partial^2\beta_x}{\partial x^2}-\frac{D_{5,1}l^2}{4R^3}\frac{\partial^4\beta_\theta}{\partial x\partial\theta^3}+\frac{D_{5,1}l^2}{4R^4}\frac{\partial^4\beta_x}{\partial\theta^4}\\
&-\frac{D_{5,1}l^2}{4R}\frac{\partial^4\beta_\theta}{\partial x^3\partial\theta}+\frac{D_{5,1}l^2}{4R^2}\frac{\partial^4\beta_x}{\partial x^2\partial\theta^2}\\
&+\frac{\partial}{\partial x}(\alpha_{11}\Delta T)D_{1,0}+\frac{\partial}{\partial x}(\alpha_{22}\Delta T)D_{3,0}-\frac{\partial N_{1,\varphi_0}}{\partial x}\\
&-\frac{\partial N_{1,\psi_0}}{\partial x}-N_{1,\varphi}\frac{\partial\varphi}{\partial x}-N_{1,\psi}\frac{\partial\psi}{\partial x}+I^{(1)}\frac{\partial^2\beta_x}{\partial t^2}+I^{(0)}\frac{\partial^2 u}{\partial t^2}=0
\end{aligned}\tag{a-19}$$

δv :

$$\begin{aligned}
&\frac{D_{5,0}l^2}{4}\frac{\partial^4 v}{\partial x^4}-D_{5,0}(\frac{l^2}{2R^2})\frac{\partial^2 v}{\partial x^2}-(D_{5,0}-C_{20})\frac{\partial^2 v}{\partial x^2}\\
&-\frac{1}{R^2}(\frac{D_{5,0}l^2}{4R^2})\frac{\partial^2 v}{\partial\theta^2}-\frac{1}{R^2}(D_{2,0}+A_{20})\frac{\partial^2 v}{\partial\theta^2}\\
&+\frac{D_{5,0}l^2}{4R^2}\frac{\partial^4 v}{\partial x^2\partial\theta^2}+\frac{1}{R^2}(\frac{D_{5,0}l^2}{4R^2}+D_{4,0}k_s)v\\
&-\frac{D_{5,0}l^2}{4R}\frac{\partial^4 u}{\partial x^3\partial\theta}-\frac{D_{5,0}l^2}{4R^3}\frac{\partial^4 u}{\partial x\partial\theta^3}+\frac{1}{R}(\frac{D_{5,0}l^2}{4R^2}-D_{3,0}-D_{5,0})\frac{\partial^2 u}{\partial x\partial\theta}\\
&+\frac{3D_{5,0}l^2}{4R^2}\frac{\partial^3 w}{\partial x^2\partial\theta}+\frac{D_{5,0}l^2}{4R^4}\frac{\partial^3 w}{\partial\theta^3}-\frac{1}{R^2}(D_{2,0}+\frac{D_{5,0}l^2}{4R^2}+D_{4,0}k_s)\frac{\partial w}{\partial\theta}\\
&-\frac{1}{R}(\frac{D_{5,0}l^2}{2R}+D_{5,1}+D_{3,1}+\frac{D_{5,1}l^2}{4R^2})\frac{\partial^2\beta_x}{\partial x\partial\theta}\\
&-\frac{1}{R^2}(\frac{D_{5,0}l^2}{4R}+D_{2,1})\frac{\partial^2\beta_\theta}{\partial\theta^2}-(\frac{3D_{5,0}l^2}{4R}+D_{5,1}+\frac{D_{5,1}l^2}{4R^2})\frac{\partial^2\beta_\theta}{\partial x^2}\\
&+\frac{D_{5,1}l^2}{4R^2}\frac{\partial^4\beta_\theta}{\partial x^2\partial\theta^2}-\frac{D_{5,1}l^2}{4R^3}\frac{\partial^4\beta_x}{\partial x\partial\theta^3}+\frac{D_{5,1}l^2}{4}\frac{\partial^4\beta_\theta}{\partial x^4}-\frac{1}{R}(\frac{D_{5,0}l^2}{4R^2}\\
&+D_{4,0}k_s)\beta_\theta-\frac{D_{5,1}l^2}{4R}\frac{\partial^4\beta_x}{\partial x^3\partial\theta}-\frac{1}{R}(\frac{\partial N_{2,\varphi_0}}{\partial\theta}+\frac{\partial N_{2,\psi_0}}{\partial\theta})\\
&-\frac{1}{R}(N_{2,\varphi}\frac{\partial\varphi}{\partial\theta}+N_{2,\psi}\frac{\partial\psi}{\partial\theta})-\frac{1}{R}(-N_{4,\varphi}\frac{\partial\varphi}{\partial\theta}-N_{4,\psi}\frac{\partial\psi}{\partial\theta})\\
&+I^{(1)}\frac{\partial^2\beta_\theta}{\partial t^2}+I^{(0)}\frac{\partial^2 v}{\partial t^2}=0
\end{aligned}\tag{b-19}$$

$\delta\beta_x$:

$$\begin{aligned}
&-(\frac{D_{5,0}l^2}{4})\frac{\partial^2\beta_x}{\partial x^2}-(D_{1,2}+A_{22})\frac{\partial^2\beta_x}{\partial x^2}+\frac{D_{5,2}l^2}{4R^2}\frac{\partial^4\beta_x}{\partial x^2\partial\theta^2}\\
&+\frac{D_{5,2}l^2}{4R^4}\frac{\partial^4\beta_x}{\partial\theta^4}-\frac{1}{R^2}(D_{5,0}l^2-\frac{D_{5,1}l^2}{2R})\frac{\partial^2\beta_x}{\partial\theta^2}\\
&-\frac{1}{R^2}(D_{5,2}+C_{22})\frac{\partial^2\beta_x}{\partial\theta^2}+(\frac{D_{5,0}l^2}{4R^2})\beta_x\\
&+(D_{5,0}k_s+C_{20})\beta_x-\frac{1}{R}(-\frac{3D_{5,0}l^2}{4}+\frac{D_{5,1}l^2}{2R})\frac{\partial^2\beta_\theta}{\partial x\partial\theta}\\
&-\frac{1}{R}(D_{3,2}+D_{5,2}+C_{22}+B_{22})\frac{\partial^2\beta_\theta}{\partial x\partial\theta}-\frac{D_{5,2}l^2}{4R^3}\frac{\partial^4\beta_\theta}{\partial x\partial\theta^3}\\
&-\frac{D_{5,2}l^2}{4R}\frac{\partial^4\beta_\theta}{\partial x^3\partial\theta}+\frac{1}{R^2}(\frac{5D_{5,0}l^2}{4R})\frac{\partial^2 u}{\partial\theta^2}-\frac{1}{R^2}(D_{5,1}+C_{21})\frac{\partial^2 u}{\partial\theta^2}\\
&-\frac{1}{R}(\frac{D_{5,0}l^2}{2R}+\frac{D_{5,1}l^2}{4R^2})\frac{\partial^2 v}{\partial x\partial\theta}-\frac{1}{R}(+D_{3,1}+D_{5,1}+C_{21}+B_{21})\frac{\partial^2 v}{\partial x\partial\theta}\\
&+\frac{D_{5,0}l^2}{4}\frac{\partial^3 w}{\partial x^3}+\frac{D_{5,0}l^2}{4R^2}\frac{\partial^3 w}{\partial x\partial\theta^2}-(\frac{D_{5,0}l^2}{4R^2})\frac{\partial w}{\partial x}\\
&-(-D_{5,0}k_s+\frac{D_{3,1}}{R}-C_{20}+\frac{1}{R}B_{21})\frac{\partial w}{\partial x}-\frac{D_{5,1}l^2}{4R^3}\frac{\partial^4 v}{\partial x\partial\theta^3}\\
&-(D_{1,1}+A_{21})\frac{\partial^2 u}{\partial x^2}+\frac{D_{5,1}l^2}{4R^4}\frac{\partial^4 u}{\partial\theta^4}+\frac{D_{5,1}l^2}{4R^2}\frac{\partial^4 u}{\partial x^2\partial\theta^2}\\
&-\frac{D_{5,1}l^2}{4R}\frac{\partial^4 v}{\partial x^3\partial\theta}-\frac{\partial M_{1,\varphi_0}}{\partial x}-\frac{\partial M_{1,\psi_0}}{\partial x}-M_{1,\varphi}\frac{\partial\varphi}{\partial x}\\
&-M_{1,\psi}\frac{\partial\psi}{\partial x}-N_{5,\varphi}\frac{\partial\varphi}{\partial x}-N_{5,\psi}\frac{\partial\psi}{\partial x}\\
&+I^{(2)}\frac{\partial^2\beta_x}{\partial t^2}+I^{(1)}\frac{\partial^2 u}{\partial t^2}=0
\end{aligned}\tag{c-19}$$

$\delta w:$

$$\begin{aligned}
&\frac{D_{5,0}l^2}{4}\frac{\partial^4 w}{\partial x^4}-D_{5,0}(\frac{l^2}{4R^2}+k_s)\frac{\partial^2 w}{\partial x^2}+\frac{D_{5,0}l^2}{2R^2}\frac{\partial^4 w}{\partial x^2\partial\theta^2}+\frac{D_{5,0}l^2}{4R^4}\frac{\partial^4 w}{\partial\theta^4}\\
&-\frac{1}{R^2}(\frac{D_{5,0}l^2}{4R^2}+D_{4,0}k_s)\frac{\partial^2 w}{\partial\theta^2}+\frac{D_{2,0}}{R^2}w+\frac{D_{3,0}}{R}\frac{\partial u}{\partial x}+\frac{D_{5,0}l^2}{2R^3}\frac{\partial^3 u}{\partial x\partial\theta^2}\\
&-\frac{3D_{5,0}l^2}{4R^2}\frac{\partial^3 v}{\partial x^2\partial\theta}+\frac{1}{R^2}(D_{2,0}+\frac{D_{5,0}l^2}{4R^2}+D_{4,0}k_s)\frac{\partial v}{\partial\theta}-\frac{D_{5,0}l^2}{4R^4}\frac{\partial^3 v}{\partial\theta^3}\\
&-\frac{D_{5,0}l^2}{4R^2}\frac{\partial^3\beta_x}{\partial x\partial\theta^2}-\frac{D_{5,0}l^2}{4}\frac{\partial^3\beta_x}{\partial x^3}+(\frac{D_{5,0}l^2}{4R^2}-D_{5,0}k_s+\frac{D_{3,1}}{R})\frac{\partial\beta_x}{\partial x}\\
&-\frac{D_{5,0}l^2}{4R^3}\frac{\partial^3\beta_\theta}{\partial\theta^3}-\frac{1}{R}(\frac{D_{5,0}l^2}{4R^2}+D_{4,0}k_s-\frac{D_{2,1}}{R})\frac{\partial\beta_\theta}{\partial\theta}\\
&-\frac{1}{2R}(\frac{D_{5,0}l^2}{2}+\frac{D_{5,1}l^2}{R})\frac{\partial^3\beta_\theta}{\partial x^2\partial\theta}-\frac{1}{R}((\alpha_{11}\Delta T)D_{3,0})\\
&-\frac{1}{R^2}(\alpha_{22}\Delta T)D_{2,0})-\frac{1}{R}(-N_{2,\varphi_0}-N_{2,\varphi}\varphi-N_{2,\psi_0}-N_{2,\psi}\psi)\\
&+\frac{1}{R}N_{4,\varphi}\frac{\partial^2\varphi}{\partial\theta^2}+\frac{1}{R}N_{4,\psi}\frac{\partial^2\psi}{\partial\theta^2}+N_{5,\varphi}\frac{\partial^2\varphi}{\partial x^2}+N_{5,\psi}\frac{\partial^2\psi}{\partial x^2}+I^{(0)}\frac{\partial^2 w}{\partial t^2}\\
&-q(x,\theta)+k_w w-k_g[\frac{1}{R^2}\frac{\partial^2 w}{\partial\theta^2}+\frac{\partial^2 w}{\partial x^2}]=0
\end{aligned}\tag{d-19}$$

$\delta\beta_\theta:$

$$\begin{aligned}
&\frac{D_{5,2}l^2}{4}\frac{\partial^4\beta_\theta}{\partial x^4}-(D_{5,0}l^2+\frac{D_{5,2}l^2}{2R^2}+\frac{D_{5,1}l^2}{2R})\frac{\partial^2\beta_\theta}{\partial x^2}\\
&-(D_{5,2}+C_{22})\frac{\partial^2\beta_\theta}{\partial x^2}+\frac{D_{5,2}l^2}{4R^2}\frac{\partial^4\beta_\theta}{\partial x^2\partial\theta^2}\\
&+\frac{D_{5,1}l^2}{4}\frac{\partial^4 v}{\partial x^4}-\frac{1}{R^2}(\frac{D_{5,0}l^2}{4})\frac{\partial^2\beta_\theta}{\partial\theta^2}-\frac{1}{R^2}(D_{2,2}+A_{22})\frac{\partial^2\beta_\theta}{\partial\theta^2}\\
&-\frac{1}{R}(-\frac{3D_{5,0}l^2}{4}+\frac{D_{5,1}l^2}{2R})\frac{\partial^2\beta_x}{\partial x\partial\theta}\\
&-\frac{1}{R}(D_{3,2}+D_{5,2}+B_{22}+C_{22})\frac{\partial^2\beta_x}{\partial x\partial\theta}-\frac{D_{5,1}l^2}{4R^3}\frac{\partial^4 u}{\partial x\partial\theta^3}\\
&-\frac{D_{5,2}l^2}{4R^3}\frac{\partial^4\beta_x}{\partial x\partial\theta^3}-\frac{D_{5,2}l^2}{4R}\frac{\partial^4\beta_x}{\partial x^3\partial\theta}\\
&-\frac{1}{R}(\frac{D_{5,0}l^2}{4R}-\frac{D_{5,1}l^2}{2R^2})\frac{\partial^2 u}{\partial x\partial\theta}\\
&-\frac{1}{R}(+D_{3,1}+D_{5,1}+B_{21}+C_{21})\frac{\partial^2 u}{\partial x\partial\theta}\\
&-(\frac{3D_{5,0}l^2}{4R}+\frac{D_{5,1}l^2}{4R^2})\frac{\partial^2 v}{\partial x^2}-(D_{5,1}+C_{21})\frac{\partial^2 v}{\partial x^2}\\
&-\frac{1}{R^2}(\frac{D_{5,0}l^2}{4R})\frac{\partial^2 v}{\partial\theta^2}-\frac{1}{R^2}(D_{2,1}+A_{21})\frac{\partial^2 v}{\partial\theta^2}\\
&-\frac{1}{R}(\frac{D_{5,0}l^2}{4R^2})v-\frac{1}{R}(C_{20}+k_sD_{4,0})v\\
&+\frac{1}{R}(\frac{D_{5,0}l^2}{4}+\frac{D_{5,1}l^2}{2R})\frac{\partial^3 w}{\partial x^2\partial\theta}\\
&+\frac{D_{5,0}l^2}{4R^3}\frac{\partial^3 w}{\partial\theta^3}+\frac{1}{R}(\frac{D_{5,0}l^2}{4R^2})\frac{\partial w}{\partial\theta}\\
&+\frac{1}{R}(+k_sD_{4,0}-\frac{D_{2,1}}{R}+C_{20}-\frac{A_{2,1}}{R})\frac{\partial w}{\partial\theta}\\
&+\frac{D_{5,1}l^2}{4R^2}\frac{\partial^4 v}{\partial x^2\partial\theta^2}-\frac{D_{5,1}l^2}{4R}\frac{\partial^4 u}{\partial x^3\partial\theta}\\
&+(\frac{D_{5,0}l^2}{4R^2})\beta_\theta+(k_sD_{4,0}+C_{20})\beta_\theta\\
&-\frac{1}{R}(\frac{\partial M_{2,\varphi_0}}{\partial\theta}+\frac{\partial M_{2,\psi_0}}{\partial\theta})-\frac{1}{R}M_{2,\varphi}\frac{\partial\varphi}{\partial\theta}\\
&-\frac{1}{R}M_{2,\psi}\frac{\partial\psi}{\partial\theta}-N_{4,\varphi}\frac{\partial\varphi}{\partial\theta}-N_{4,\psi}\frac{\partial\psi}{\partial\theta}+I^{(1)}\frac{\partial^2 v}{\partial t^2}\\
&+I^{(2)}\frac{\partial^2\beta_\theta}{\partial t^2}=0
\end{aligned}\tag{e-19}$$

$\delta\varphi:$

$$\begin{aligned}
&N_{5,\varphi}(\frac{\partial^2 w}{\partial x^2}+\frac{\partial\beta_x}{\partial x})+N_{1,D}\frac{\partial^2\varphi}{\partial x^2}\\
&+N_{1,B}\frac{\partial^2\psi}{\partial x^2}+N_{4,\varphi}(\frac{1}{R}\frac{\partial^2 w}{\partial\theta^2}+\frac{\partial\beta_\theta}{\partial\theta}-\frac{1}{R}\frac{\partial v}{\partial\theta})\\
&+N_{2,B}\frac{\partial^2\varphi}{\partial\theta^2}+N_{2,D}\frac{\partial^2\psi}{\partial\theta^2}\\
&+N_{1,\varphi}\frac{\partial u}{\partial x}+M_{1,\varphi}\frac{\partial\beta_x}{\partial x}+\frac{1}{R}N_{2,\varphi}(w+\frac{\partial v}{\partial\theta})\\
&+M_{2,\varphi}\frac{\partial\beta_\theta}{\partial\theta}-N_{3,D1}\varphi_0-N_{3,D}\varphi\\
&-N_{3,B1}\varphi_0-N_{3,B}\varphi=0
\end{aligned}\tag{f-19}$$

$\delta\psi_2:$

$$\begin{aligned}
&N_{5,\psi}(\frac{\partial^2 w_2}{\partial x^2}+\frac{\partial\beta_{x2}}{\partial x})+N_{1,B}\frac{\partial^2\varphi_2}{\partial x^2}\\
&+N_{1,B1}\frac{\partial^2\psi_2}{\partial x^2}+N_{4,\psi}(\frac{1}{R}\frac{\partial^2 w_2}{\partial\theta^2}+\frac{\partial\beta_{\theta2}}{\partial\theta}-\frac{1}{R}\frac{\partial v_2}{\partial\theta})\\
&+N_{2,D}\frac{\partial^2\varphi_2}{\partial\theta^2}+N_{2,B1}\frac{\partial^2\psi_2}{\partial\theta^2}\\
&+N_{1,\psi}\frac{\partial u_2}{\partial x}+M_{1,\psi}\frac{\partial\beta_{x2}}{\partial x}\\
&+\frac{1}{R}N_{2,\psi}(w_2+\frac{\partial v_2}{\partial\theta})+M_{2,\psi}\frac{\partial\beta_{\theta2}}{\partial\theta}\\
&-N_{3,B1}\varphi_0-N_{3,B}\varphi_2-N_{3,D2}\psi_0-N_{3,B2}\psi_2=0
\end{aligned}\tag{g-19}$$

3. Solving method

Navier's type solution is employed for simply supported boundary conditions of the micro sandwich cylindrical shell as follows:

$$\begin{aligned}
u(x,\theta,t)&=\sum_{m=1}^{\infty}\sum_{n=1}^{\infty}U_m\cos(\frac{m\pi x}{L})\cos(n\theta)e^{i\omega t}\\
v(x,\theta,t)&=\sum_{m=1}^{\infty}\sum_{n=1}^{\infty}V_m\sin(\frac{m\pi x}{L})\sin(n\theta)e^{i\omega t}\\
w(x,\theta,t)&=\sum_{m=1}^{\infty}\sum_{n=1}^{\infty}W_m\sin(\frac{m\pi x}{L})\cos(n\theta)e^{i\omega t}\\
\beta_x(x,\theta,t)&=\sum_{m=1}^{\infty}\sum_{n=1}^{\infty}\beta_x\cos(\frac{m\pi x}{L})\cos(n\theta)e^{i\omega t}\\
\beta_t(x,\theta,t)&=\sum_{m=1}^{\infty}\sum_{n=1}^{\infty}\beta_t\cos(\frac{m\pi x}{L})\cos(n\theta)e^{i\omega t}\\
\varphi(x,\theta,t)&=\sum_{m=1}^{\infty}\sum_{n=1}^{\infty}\varphi_m\sin(\frac{m\pi x}{L})\cos(n\theta)e^{i\omega t}\\
\psi(x,\theta,t)&=\sum_{m=1}^{\infty}\sum_{n=1}^{\infty}\psi_m\sin(\frac{m\pi x}{L})\cos(n\theta)e^{i\omega t}
\end{aligned}\tag{20}$$

where m and n are half axial and peripheral wave numbers, respectively.

In the matrix form:

$$\left\{\left[K\right]-\left[M\right]\omega^2\right\}\left\{U\right\}=0$$
$$\left\{U\right\}=\left\{U_m \quad V_m \quad W_m \quad \beta_x \quad \beta_t \quad \varphi_m \quad \psi_m\right\}^T \tag{21}$$

where [K], [M] and {U}are stiffness matrix, mass matrix and displacement vector, respectively.

4. Numerical result and discussion

In order to ensure the obtained results for the free vibration analysis of Cooper-Naghdi micro sandwich cylindrical shell with saturated porous core and reinforced carbon nanotube piezoelectric composite face sheets, they are compared with other researches in Tables 3-5. The dimensionless natural frequencies of micro composite sandwich cylindrical shell ($\overline{\omega} = \omega R\sqrt{\rho(1-\nu_{12}^2)/E_{11}}$) based on classical theory (without any small scale parameter, ($l = 0$) and modified couple stress theory ($l \neq 0$) are reported in Table 3. The dimensionless natural frequencies of piezoelectric cylindrical nanoshell are reported in Table 4. The dimensionless natural frequencies of porous cylindrical nanoshell with uniform distribution are listed in Table 5. For three tables, the obtained results have a good agreement with literature results.

The effects of various parameters such as SWCNT volume fraction, length to thickness ratio, temperature change, porosity distribution, small scale coefficient, the face sheet thickness to the core thickness ratio, foundation constants on the natural frequency of Cooper-Naghdi micro sandwich cylindrical shell with saturated porous core and reinforced CNT piezoelectric composite face sheets based on the modified coupling stress theory are studied.

Table 3 The dimensionless natural frequencies of micro composite sandwich cylindrical shell based on classic theory *(l = 0)* and modified couple stress theory ($\overline{\omega} = \omega R\sqrt{\rho(1-\nu_{12}^2)/E_{11}}$

h / R	n	(Mohammadimehr and Mehrabi (2017) (l= 0)	Present work (l= 0)	Error (%)	(Mohammadimehr and Mehrabi (2017) (l= 17.6 μm)	present work (MCST)	Error (%)
0.1	1	0.934	0.932	0.21	1.116	1.119	0.27
0.1	2	0.777	0.774	0.39	1.054	1.056	0.19
0.2	1	1.049	1.039	0.95	1.525	1.489	2.36
0.2	2	0.971	0.951	2.06	1.574	1.527	2.99
0.3	1	1.181	1.152	2.46	1.875	1.782	4.96
0.3	2	1.163	1.110	4.56	1.964	1.866	4.99

Table 4 The dimensionless natural frequencies of piezoelectric cylindrical nanoshell

n	Ke *et al*. (2015)	present	Error (%)	Loy *et al*. (1997)	Error (%)
1	0.0168	0.0158	1.37	0.0161	1.4
2	0.00938	0.00936	0.2	0.00938	0.2
3	0.02210	0.02209	0.08	0.02210	0.06
4	0.04209	0.04206	0.09	0.04209	0.08

Table 5 The dimensionless natural frequencies of porous cylindrical nanoshell with uniform distribution

n	Wang and Wu (2017)	present	Error (%)
1	0.0161	0.0168	4.3
2	0.0094	0.0096	2.12
3	0.0221	0.0222	0.45
4	0.0421	0.0423	0.47
5	0.0680	0.0683	0.44

Geometric and mechanical properties are taken as follows (Farajpour *et al*. (2016)):

For matrix of face sheet ($BiTiO_3$– $CoFe_2O_4$):

$elastic\ \ cons\tan ts$

$C_{11}=C_{22}=226MPa, C_{12}=125MPa, C_{13}=124MPa, C_{33}=216MPa$

$C_{44}=C_{55}=44.2MPa, C_{66}=50.5MPa,$

$piezoelectric\ \ cons\tan ts$

$e_{31}=e_{32}=-2.2C/m^2, e_{15}=e_{24}=5.8C/m^2, e_{33}=9.3C/m^2,$

$piezomagnetic\ \ cons\tan ts$

$q_{31}=q_{32}=290.1H/\text{m}, q_{15}=q_{24}=275H/\text{m}, q_{33}=349.9H/\text{m},$

$dielectric\ \ cons\tan ts$

$\text{K}_{11}=\text{K}_{22}=5.64, \text{K}_{33}=6.35,$

$magnetoelectric\ \ cons\tan ts$

$g_{11}=g_{22}=5.367V/m.Oe, g_{33}=2737.5V/m.Oe,$

$magnetic\ \ cons\tan ts$

$\mu_{11}=\mu_{22}=-297N/A^2, \mu_{33}=53.5N/A^2,$

other

$\rho=5550kg/m^3, \alpha=4.74\text{e}-51/K, \nu=0.25, \text{h}=2\mu\text{m},$

$\text{l}=17.6\mu\text{m}, \text{L}=20\text{h}, \text{K}_W=600\text{GN/m}^3, \text{K}_\text{G}=1000\text{N/m}$

Fig. 3 depicts first four dimensionless natural frequencies of micro sandwich cylindrical shell with saturated porous core and reinforced carbon nanotube piezoelectric composite face sheets for a- radius to thickness ratio (*R / t*) b- length to radius ratio (*L / R*). As the figure shows, with the increase in radius to the thickness ratio of the micro-shell, the dimensionless natural frequency of the system increases. In the other words, in higher modes and same radii to the thickness ratio, the natural frequency is greater. It can also be seen that as this ratio increases, the non-dimensional natural frequency increases.

Under the same conditions, by increasing length to the radius ratio of the micro-shell, the dimensionless natural frequencies for different modes are examined (Fig. 3-b). As it can be seen, the natural frequencies of the system decrease with increasing of this ratio, particularly in higher modes.

Fig. 4 illustrates the effect of the small scale coefficient on the dimensionless natural frequencies of the micro sandwich cylindrical shell. As it is shown in the figure, the dimensionless natural frequency increases and this increase is more in higher modes.

In Fig. 5, the effect of volume fraction of SWCNTs has been shown. It is expected that with adding SWCNTs to the micro sandwich cylindrical shell, rigidity of the structure increases leads to enhance the dimensionless natural frequency.

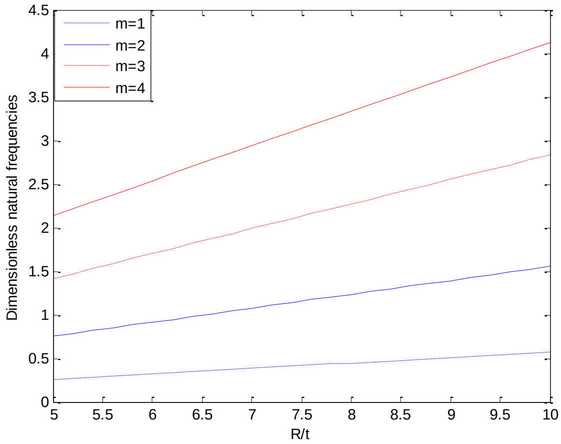

a-

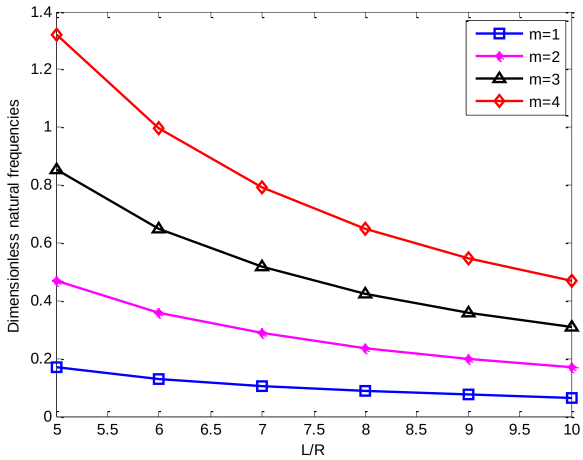

b-

Fig. 3 First four dimensionless natural frequencies of the micro sandwich cylindrical shell with saturated porous core and reinforced carbon nanotube piezoelectric composite face sheets for a- radius to thickness ratio b- length to radius ratio

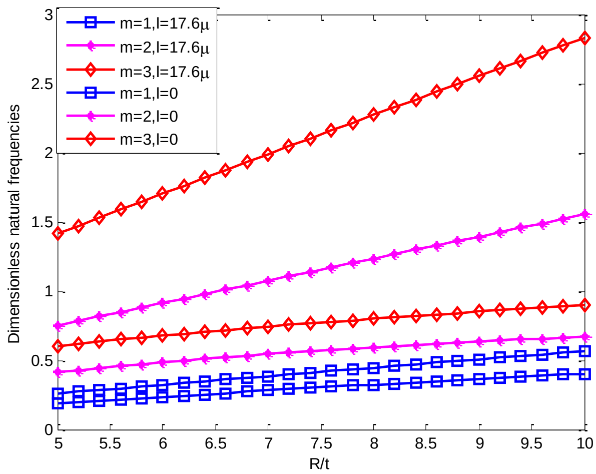

Fig. 4 The effect of the small-scale coefficient on the dimensionless natural frequency of the micro sandwich cylindrical shell

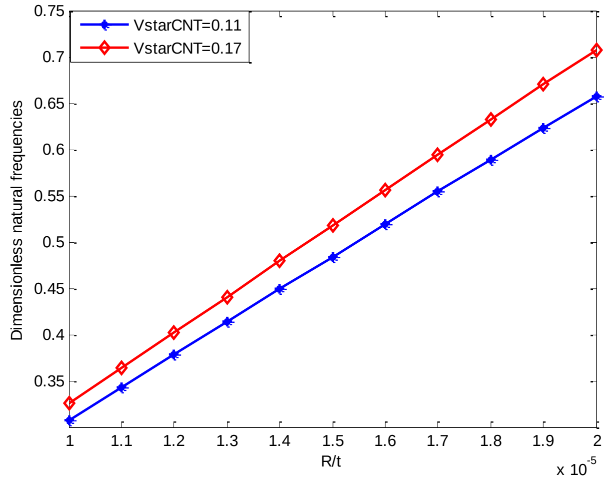

Fig. 5 Effect of SWCNT volume fraction on the dimensionless natural frequencies of the micro sandwich cylindrical shell

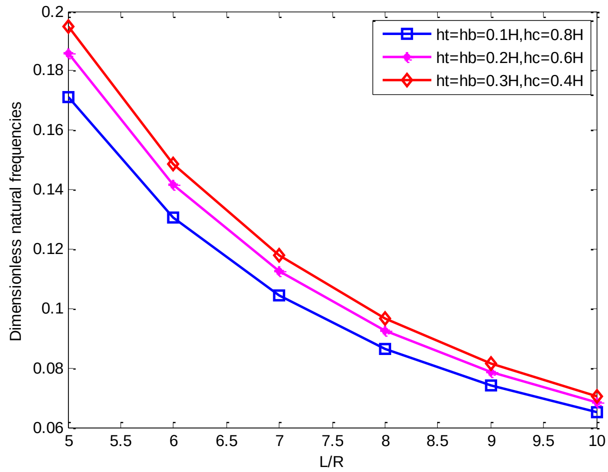

a-

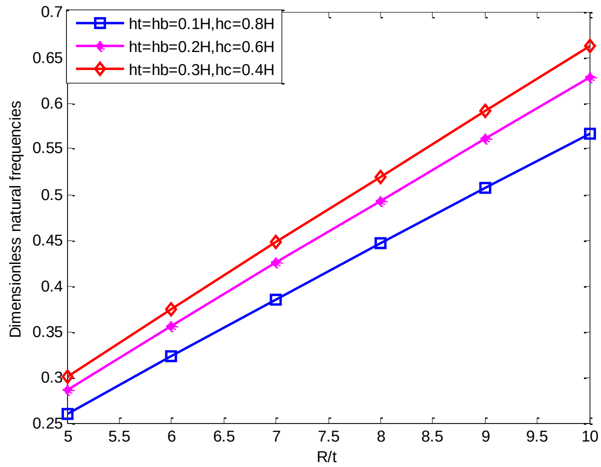

b-

Fig. 6 Effect of thickness ratio on the dimensionless natural frequencies of the micro sandwich cylindrical shell for a- length to radius ratio b- radius to thickness ratio

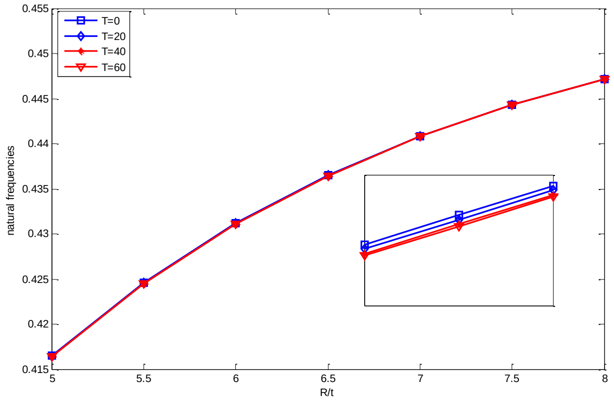

Fig. 7 Effect of temperature rise on the dimensionless natural frequencies of the micro sandwich cylindrical shell

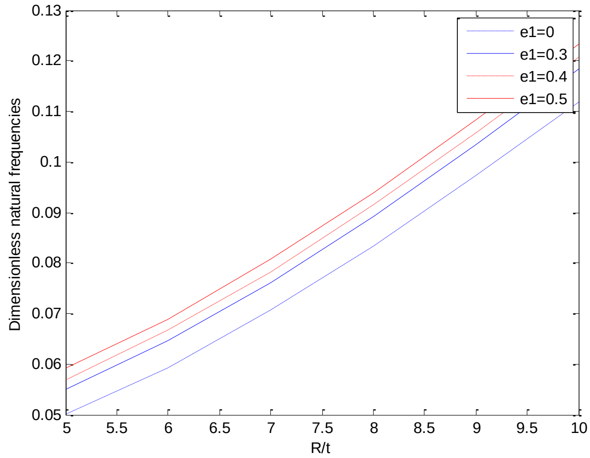

Fig. 8 Effect of porosity coefficient on the dimensionless natural frequencies of the micro sandwich cylindrical shell

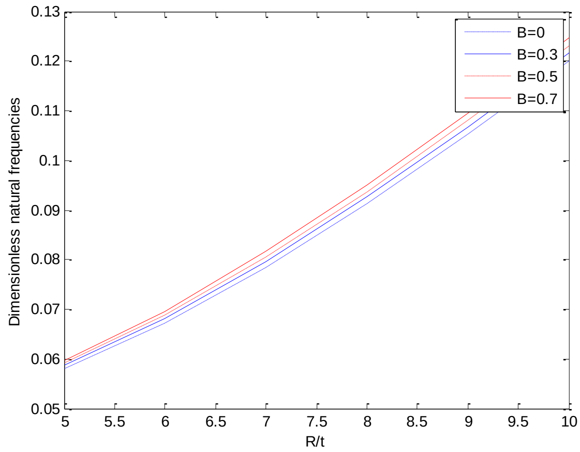

Fig. 9 Effect of Skempton coefficient on the dimensionless natural frequencies of the micro sandwich cylindrical shell

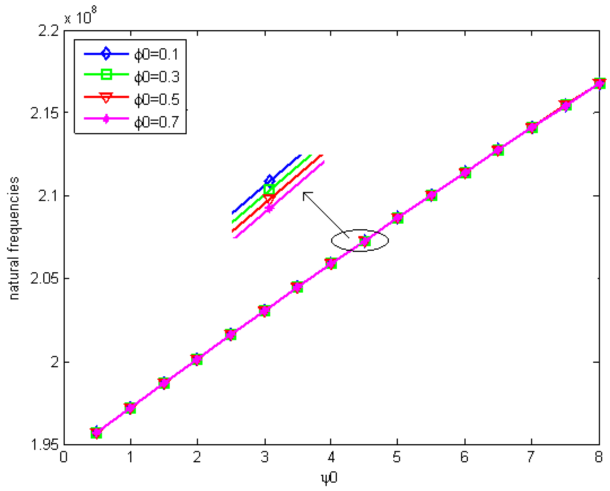

Fig. 10 The natural frequencies of the micro sandwich cylindrical shell versus magnetic field

Figs. 6-a and b display the natural frequencies of the micro sandwich cylindrical shell for radius to thickness ratio (R / t) b- length to radius ratio (L / R) and different face sheet thickness to core thickness ratio (h_t /h_c). Total thickness of the micro sandwich cylindrical shell is considered constant. As the face sheet thickness is higher than the core thickness, the natural frequency is greater.

The effect of temperature change on the dimensionless natural frequencies of the micro sandwich cylindrical shell is shown in Fig. 7. It can be seen that as the temperature rises, the natural frequency and the stiffness of the micro sandwich cylindrical shell decreases.

Increasing the porosity coefficient and radius to thickness ratio (R / t) lead to enhance the natural frequency of the micro sandwich cylindrical shell, as shown in the Fig. 8 that this increase is more in the higher porosity coefficient. As the porosity increases, the free space volume of the micro sandwich cylindrical shell increases, and the weight of the structure decreases, as well as its stiffness. But the effect of the structure's stiffness is higher, so the frequency of the structure increases with increasing porosity.

According to the Fig. 9, as the porosity coefficient, the increase in Skempton coefficient increases the natural frequency.

Fig. 10 shows the magnetic field and applied voltage effects on the natural frequency of the micro sandwich cylindrical shell. As it can be observed from this figure, the natural frequency raises with presence of magnetic and voltage applying. Also, effect of magnetic field on the natural frequency is higher than applied voltage.

7. Conclusion

Free vibration of the Cooper-Naghdi micro sandwich cylindrical shell with saturated porous core and reinforced carbon nanotube piezoelectric composite face sheets under magneto-hydro-thermo-mechanical loadings was investigated. Modified couple stress theory was used for considering small scale effect. The governing equations were obtained by Hamilton’s principle and the natural frequencies are derived using Navier’s method. The following results are obtained:

• With an increase in the radius to thickness ratio of the micro sandwich cylindrical shell results, the natural frequency particularly increases.

• Increasing of the length to radius ratio for the micro sandwich cylindrical shell decreases the natural frequency.

• Increasing of the face sheet thickness of the micro sandwich cylindrical shell with porous core, increases the natural frequency.

• Enhancing of the porosity of the core for the micro sandwich cylindrical shell, enhances the natural frequency.

• The natural frequency of the micro sandwich cylindrical shell increases with increasing of skempton coefficient.

• Adding carbon nanotubes to the micro sandwich cylindrical shell enhances the stiffness of the structure.

• An increase in temperature in the micro sandwich cylindrical shell causes a decrease in the natural frequency.

• Applying magnetic and voltage fields strengthen the micro sandwich cylindrical shell.

Acknowledgment

The authors would like to thank the referees for their valuable comments. Also, they are thankful to the Iranian Nanotechnology Development Committee for their financial support and the University of Kashan for supporting this work by Grant No. 682561/7.

References

Akbari Alashti, R. and Khorsand, M. (2012), “Tree-dimensional dynamo-thermo-elastic of a functionally graded cylindrical shell with piezoelectric layers by DQ-FD coupled”, *J. Pres. Vessels Piping*, **96-97**, 49-67. https://doi.org/10.1016/j.ijpvp.2012.06.006.

Ansari, R., Gholami, R. and Sahmani, S. (2011), “Free vibration analysis of size-dependent functionally graded microbeams based on the strain gradient Timoshenko beam theory”, *Compos. Struct.*, **94**, 221-228. https://doi.org/10.1016/j.compstruct.2011.06.024.

Arani, A.G. and Amir, S. (2013), “Electro-thermal vibration of visco-elastically coupled BNNT systems conveying embedded on elastic foundation via strain gradient theory”, *Physica B Condense Matt.*, **419**, 1-6. https://doi.org/10.1016/j.physb.2013.03.010.

Arani, A.G., Arani, H.K. and Maraghi, Z.K. (2016), “Vibration analysis of sandwich composite micro-plate under electro-magneto-mechanical loadings”, *Appl. Math. Model*. **40**, 10596-10615. https://doi.org/10.1016/j.apm.2016.07.033.

Arani, A.G., Haghparast, E., Maraghi, Z.K. and Amir, S. (2015), “Static stress analysis of carbon nano-tube reinforced composite (CNTRC) cylinder under non-axisymmetric thermo-mechanical loads and uniform electromagnetic fields”, Compos. Part B Eng., **68**, 136-145. https://doi.org/10.1016/j.compositesb.2014.08.036.

Arani, A.G., Mobarakeh, M.R., Shams, S. and Mohammadimehr, M. (2012), “The effect of CNT volume fraction on the magneto-thermo-electro-mechanical behavior of smart nanocomposite cylinder”, *J. Mech. Sci, Tech.*, **26**(8), 2565-2572. https://doi.org/10.1007/s12206-012-0639-5.

Arani, A.G., Rousta Navi, B. and Mohammadimehr, M. (2016), “Surface stress and agglomeration effects on nonlocal biaxial buckling polymeric nanocomposite plate reinforced by CNT using various approaches”, Adv. Compos. Mater., **25**(5), 423-441. https://doi.org/10.1080/09243046.2015.1052189.

Arefi, M. and Zenkour, A.M. (2016), “Vibration and bending analysis of a sandwich microbeam with two integrated piezo-magnetic face-sheets”, *Compos. Struct.*,**159**, 479-490. https://doi.org/10.1016/j.compstruct.2016.09.088.

Bahadori, R. and Najafizadeh, M.M. (2015), “Free vibration of two-dimensional functionally graded axisymmetric cylindrical shell on Winkler-Pasternak elastic foundation by First-order Shear Deformation Theory and using Navier differential quadrature solution methods”, *Appl. Math. Model*, **39**, 4877-4894. https://doi.org/10.1016/j.apm.2015.04.012.

Chen, N., Long, C., Li, Y., Wang, D. and Zhu, H. (2018), “High-performance layered double hydroxide/poly(2,6-dimethyl-1,4-phenylene oxide) membrane with porous sandwich structure for anion exchange membrane fuel cell applications”, *J. Mem. Sci*. **552**, 51-60. https://doi.org/10.1016/j.memsci.2018.01.045.

Cooper, R.M. and Naghdi, P.M. (1957), “Propagation of non-axially symmetric waves in elastic cylindrical shells”, *J. Acous. Soc. Am*., **29**, 1365-1372. https://doi.org/10.1121/1.1908812

Dehrouyeh-Semnani, A.M., Dehrouyeh, M., Torabi-Kafshgari, M. and Nikkhah-Bahrami, M.A. (2015), “Damped sandwich beam model based on symmetric-deviatoric couple stress theory”, *J. Eng. Sci*., **92**, 83-94. https://doi.org/10.1016/j.ijengsci.2015.03.007.

Dey, T. and Ramachandra, L.S (2016), “Non-Linear vibration analysis of laminated composite circular cylindrical shells”, *Compos. Struct.*, **163**, 89-100. https://doi.org/10.1016/j.compstruct.2016.12.018.

Dong, Y.H. and Li, Y.H. (2016), “A unified nonlinear analytical solution of bending buckling and vibration for the temperature-dependent FG rectangular plates subjected to thermal load”, *Compos. Struct.*, **159**, 689-701. https://doi.org/10.1016/j.compstruct.2016.10.001.

Farajpour, A., Hairi Yazdi, M.R., Rastgoo, A., Loghmani, M. and Mohammadi, M. (2016), “Nonlocal nonlinear plate model for large amplitude vibration of magneto-electro-elastic nanoplate”, *Compos. Struct*., **140**, 323-336. https://doi.org/10.1016/j.compstruct.2015.12.039.

Gui, W., Liang, Y., Hao, G., Lin, J., Sun, D., Liu, M., Liu, C. and Zhang, H. “High Nb-TiAl-based porous composite with hierarchical micro-pore structure for high temperature applications”, https://doi.org/10.1016/j.jallcom.2018.02.081.

Jabbari, M., Farzaneh Joubaneh, E., Khorshidvand, A.R. and Eslami, M.R. (2013), “Buckling analysis of porous circular plate with piezoelectric actuator layers under uniform radial compression”, *Int. J. Mech. Sci*., **70**, 50-56. https://doi.org/10.1016/j.ijmecsci.2013.01.031.

Jalaei, M.H. and Arani, A.G. (2018), “Size-dependent static and dynamic responses of embedded double-layered graphene sheets under longitudinal magnetic field with arbitrary boundary conditions”, *Compos. Part B*, **142**, 117-130. https://doi.org/10.1016/j.compositesb.2017.12.053.

Kamarian, S. and Shakeri, M. (2016), “Natural frequency analysis of composite skew plates with embedded shape memory alloys in thermal environment”, *Int. J. Mech. Sci*., **108**, 157-165.

Ke, L.L., Liu, C.H. and Wang, Y. (2015), “Free vibration of nonlocal piezoelectric nanoplates under various boundary conditions”, *Physica E*., **66**, 93-106. https://doi.org/10.1016/j.physe.2014.10.002.

Kheibari, K. and Tadi Beni, Y. (2016), “Size dependent electromechanical vibration of single-walled piezoelectric nanotubes using thin shell model”, *Mater. Des.*, **114**, 572-583. https://doi.org/10.1016/j.matdes.2016.10.041.

Lee, J., Lee, Y. A., Yoo, C. Y., Yoo, J. J., Gwak, R., Cho, W. K., Kim, B. and Yoon, H. (2018), "Self-templated synthesis of interconnected porous carbon nanosheets with controllable pore size: Mechanism and electrochemical capacitor application.", *Micro. Meso. Mater.*, **261**, 119-125. https://doi.org/10.22060/mej.2017.12655.5389.

Lei, Z.X., Zhang, L.W. and Liew, K.M. (2015), "Vibration analysis of CNT-reinforced functionally graded rotating cylindrical panels using the element-free kp-Ritz method", Compos. Part B, **77**, 291-303. https://doi.org/10.1016/j.compositesb.2015.03.045

Li, Y.S. and Pan, E. "Static bending and free vibration of a functionally graded piezoelectric microplate based on the modified couple-stress theory", *Int. J. Eng. Sci.*, **97**, 40-59. https://doi.org/10.1016/j.ijengsci.2015.08.009.

Loy, C.T., Lam, K.Y. and Shu, C. (1997), "Analysis of cylindrical shells using generalized differential quadrature", *Shock Vib*., **4,** 193-198. https://doi.org/10.3233/SAV-1997-4305.

Mohammadimehr, M. and Alimirzaei, S. (2016), "Nonlinear static and vibration analysis of Euler-Bernoulli composite beam model reinforced by FG-SWCNT with initial geometrical imperfection using FEM", *Struct. Eng. Mech.*, **59**(3), 431-454. http://doi.org/10.12989/sem.2016.59.3.431.

Mohammadimehr, M. and Mehrabi, M. (2017), "Stability and free vibration analysis of double-bonded micro composite sandwich cylindrical shells conveying fluid flow", *Appl. Math Model*, **47**, 685-709. https://doi.org/10.1016/j.apm.2017.03.054.

Mohammadimehr, M. and Mostafavifar, M. (2016), "Free vibration analysis of sandwich plate with a transversely flexible core and FG-CNTs reinforced nanocomposite face sheets subjected to magnetic field and temperature-dependent material properties using SGT", *Compos Part B*, **94**, 253-270. https://doi.org/10.1016/j.compositesb.2016.03.030.

Mohammadimehr, M. and Rahmati, A.H. (2013), "Small scale effect on electro-thermo-mechanical vibration analysis of single-walled boron nitride nanorods under electric excitation", *Turk. J. Eng. Environ. Sci*., **37**(1), 1-15. https://doi.org/10.3906/muh-1201-17

Mohammadimehr, M. and Shahedi, S. (2016), "High-order buckling and free vibration analysis of two types sandwich beam including AL or PVC-foam flexible core and CNTs reinforced nanocomposite face sheets using GDQM", *Compos. Part B*, **108**, 91-107. https://doi.org/10.1016/j.compositesb.2016.09.040

Mohammadimehr, M., Okhravi, S.V. and Akhavan Alavi, S.M. (2018a), "Free vibration analysis of magneto-electro-elastic cylindrical composite panel reinforced by various distributions of CNTs with considering open and closed circuits boundary conditions based on FSDT", *J. Vib. Control*, **24**(8), 1551-1569. https://doi.org/10.1177/1077546316664022.

Mohammadimehr, M., Rostami, R. and Arefi, M. (2016d), "Electro-elastic analysis of a sandwich thick plate considering FG core and composite piezoelectric layers on Pasternak foundation using TSDT", *Steel Compos. Struct.*, **20**(3), 513-543. https://doi.org/10.12989/scs.2016.20.3.513

Mohammadimehr, M., Rousta Navi, B. and Ghorbanpour Arani, A. (2016b), "Free vibration of viscoelastic double-bonded polymeric nanocomposite plates reinforced by FG-SWCNTs using MSGT sinusoidal shear deformation theory and meshless method", *Compos. Struct.*, **131**, 654-671. https://doi.org/10.1016/j.compstruct.2015.05.077.

Mohammadimehr, M., Rousta Navi, B. and Ghorbanpour Arani, A. (2016c), "Modified strain gradient Reddy rectangular plate model for biaxial buckling and bending analysis of double-coupled piezoelectric polymeric nanocomposite reinforced by FG-SWNT", *Compos. Part B*, **87**,132-148. https://doi.org/10.1016/j.compositesb.2015.10.007

Mohammadimehr, M., Saidi, A.R., Ghorbanpour Arani, A., Arefmanesh, A. and Han, Q. (2011), "Buckling analysis of double-walled carbon nanotubes embedded in an elastic medium under axial compression using non-local Timoshenko beam theory", *Proceedings of the Institution of Mechanical Engineers, Part C J. Mech. Eng. Sci.*, **225**(2), 498-506. https://doi.org/10.1177/2041298310392861

Mohammadimehr, M., Salemi, M. and Rousta Navi, B. (2016a), "Bending buckling and free vibration analysis of MSGT microcomposite Reddy plate reinforced by FG-SWCNTs with temprature-dependent material properties under hydro-thermo-mechanical loadings using DQM", *Compos. Struct.*, **138**, 361-380. https://doi.org/10.1016/j.compstruct.2015.11.055

Mohammadimehr, M., Shabani Nejad, E. and Mehrabi, M. (2018b), "Buckling and vibration analyses of MGSGT double-bonded micro composite sandwich SSDT plates reinforced by CNTs and BNNTs with isotropic foam & flexible transversely orthotropic cores", *Struct. Eng. Mech.*, **65**(4), 491-504. https://doi.org/10.12989/sem.2018.65.4.491.

Mohammadimehr, M., Zarei, H.B., Parakandeh, A. and Arani, A.G. (2017), "Vibration analysis of double-bonded sandwich microplates with nanocomposite facesheets reinforced by symmetric and un-symmetric distributions of nanotubes under multi physical fields", *Struct. Eng. Mech*., **64**(3), 361-379. http://doi.org/10.12989/sem.2017.64.3.361.

Murmu, T., McCarthy, M.A. and Adhikari, S. (2012), "Vibration response of double-walled carbon nanotubes subjected to an externally applied longitudinal magnetic field: A nanlocal elasticity approach", *J. Sound. Vib*., **331**, 5069-5086. https://doi.org/10.1016/j.compositesb.2016.06.028

Pourasghar, A. and Kamarian, S. (2016), "Thermoelastic response of CNT reinforced cylindrical panel resting on elastic foundation using theory of elasticity", *Mater. Des*., **49**, 583-590.

Razavi, H., Babadi, A.F. and Beni, Y.T. (2017), "Free vibration analysis of functionally graded piezoelectric cylindrical nanoshell based on consistent couple stress theory", *Compos. Struct.*, **160**, 1299-1309. https://doi.org/10.1016/j.compstruct.2016.10.056

Shaat, M. (2015), "Effects of grain size and microstructure rigid rotations on the bending behavior of nanocrystalline material beams", *J. Mech. Sci*., **94-95**, 27-35. https://doi.org/10.1016/j.compositesb.2017.10.032

Shaat, M. (2015), "Physical and mathematical representations of couple stress effects on micro/nanosolids", *Int. J. Appl. Mech*., **7**(1), 155-183. https://doi.org/10.1142/S1758825115400128.

Shaat, M. and Abdelkefi, A. (2015), "Modeling the material structure and couple stress effects of nanocrystalline silicon beams for pull-in and bio-mass sensing applications", *J. Mech. Sci.*, **101-102**, 280-291. https://doi.org/10.1016/j.ijmecsci.2015.08.002

Shaat, M. and Mohamed, S.A. (2014), "Nonlinear-electrostatic analysis of micro-actuated beams based on couple stress and surface elasticity theories", *J. Mech. Sci*., **84**, 208-217. https://doi.org/10.1016/j.ijmecsci.2014.04.020

Shaat, M., Mahmoud, F.F., Gao, X.L. and Faheem, A.F. (2014), "Size-dependent bending analysis of Kirchhoff nano-plates based on a modified couple-stress theory including surface effects", *J. Mech. Sci*., **79**, 31-37. https://doi.org/10.1016/j.ijmecsci.2013.11.022

Shen, H.S., Xiang, Y., Fan, Y. and Hui, D. (2018), "Nonlinear vibration of functionally graded graphene-reinforced composite laminated cylindrical panels resting on elastic foundations in thermal environments", *Compos. Part B,* **136**, 177-186.

Song, Z.G., Zhang, L.W. and Liew, K.M. (2016), "Vibration analysis of CNT-reinforced functionally graded composite cylindrical shells in thermal environments", *J. Mech. Sci*., **115**, 339-347. https://doi.org/10.1016/j.ijmecsci.2016.06.020

Tadi Beni, Y., Mehralian, F. and Razavi, H. (2015), "Free vibration analysis of size-dependent shear deformation functionally graded cylindrical shell on the basis of modified couple stress theory", *Compos. Struct*., **120**, 65-78. https://doi.org/10.1016/j.compstruct.2014.09.065
Tsiatas, G.C. (2009), "A new Kirchhoff plate model based on a modified couple stress theory", *J. Solids. Struct*., **46**, 2757-2764. https://doi.org/10.1016/j.ijsolstr.2009.03.004
Wang, Y. and Wu, D. (2017), "Free vibration of functionally graded porous cylindrical shell using a sinusoidal shear deformation theory", *Aero Sci. Technol*., **66**, 83-91. https://doi.org/10.1016/j.ast.2017.03.003
Yang, F., Chong, A.C.M., Lam, D.C.C. and Tong, P. (2002), "Couple stress based strain gradient theory for elasticity", *J. Solids Struct*., **39**, 2731-2743. https://doi.org/10.1016/S0020-7683(02)00152-X
Yang, G. and Park, S.J. (2018), "MnO2 and biomass-derived 3D porous carbon composites electrodes for high performance supercapacitor applications", *J. Alloys Compounds*, **741**, 360-367. https://doi.org/10.1016/j.jallcom.2018.01.108.
Yang, J., Xiong, J., Ma, L., Zhang, G., Wang, X. and Wu, L. (2014), "Study on vibration damping of composite sandwich cylindrical shell with pyramidal truss-like cores", *Compos. Struct*., **117**, 362-372. https://doi.org/10.1016/j.compstruct.2014.06.042
Zeighampour, H. and Tadi Beni, Y. (2014), "Cylindrical thin-shell model based on modified strain gradient theory", *J. Eng. Sci*., **2 78**, 27-47. https://doi.org/10.1016/j.ijengsci.2014.01.004
Zhang, Q., Hu, Z., Yang, Y., Zhang, Z., Wang, X., Yang, X., An, Y. and Guo, B. (2018), "Metal organic frameworks-derived porous carbons/ruthenium oxide composite and its application in super capacitor", *J. Alloys Compounds*, **735**, 1673-1681. https://doi.org/10.1016/j.jallcom.2017.11.268
Zhang, Y. and Park, S.J. (2017), "Au–pd bimetallic alloy nanoparticle-decorated BiPO4 nanorods for enhanced photocatalytic oxidation of trichloroethylene", *J. Catalysis*, **355**, 1-10. https://doi.org/10.1016/j.jcat.2017.08.007
Zhang, Y. and Park, S.J. (2017a), "Au-pd bimetallic alloy nanoparticle-decorated BiPO4 nanorods for enhanced photocatalytic oxidation of trichloroethylene", *J. Catal*., **355**, 1-10. https://doi.org/10.1016/j.jcat.2017.08.007
Zhang, Y. and Park, S.J. (2017b), "Incorporation of RuO2 into charcoal-derived carbon with controllable microporosity by CO2 activation for high-performance supercapacitor", *Carbon*, **122**, 287-297. https://doi.org/10.1016/j.carbon.2017.06.085
Zhang, Y. and Park, S.J. (2017c), "Incorporation of RuO2 into charcoal-derived carbon with controllable microporosity by CO2 activation for high-performance supercapacitor", *Carbon*, **122**, 287-297. https://doi.org/10.1016/j.carbon.2017.06.085.
Zhang, Y. and Park, S.J. (2018), "Bimetallic AuPd alloy nanoparticles deposited on MoO3 nanowires for enhanced visible-light driven trichloroethylene degradation", *J. Catalysis*, **361**, 238-247. https://doi.org/10.1016/j.jcat.2018.03.010
Zhang, Y. and Park, S.J. (2018), "Formation of hollow MoO3/SnS2 heterostructured nanotubes for efficient light-driven hydrogen peroxide production", *J. Mater. Chem. A*, **6**, 20304-20312. https:// doi.org 10.1039/C8TA08385A.
Zhang, Y. and Park, S.J. (2018a), "Bimetallic AuPd alloy nanoparticles deposited on MoO3 nanowires for enhanced visible-light driven trichloroethylene degradation", *J. Catal.*, **361**, 238-247. https://doi.org/10.1016/j.jcat.2018.03.010
Zhang, Y. and Park, S.J. (2018b), "Formation of hollow MoO3/SnS2 heterostructured nanotubes for efficient light-driven hydrogen peroxide production", *J. Mater. Chem. A*, **6**, 20304-20312. https://doi.org/10.1039/C8TA08385A.
Zhang, Y. and Park, S.J. (2019), "Facile construction of MoO3@ZIF-8 core-shell nanorods for efficient photoreduction of aqueous Cr (VI)", *Catal B Environ*., **240**, 92-10. https://doi.org/10.1016/j.apcatb.2018.08.077
Zhang, Y. and Park, S.J. (2019), "Facile construction of MoO3@ZIF-8 core-shell nanorods for efficient photoreduction of aqueous Cr (VI)", *Appl. Catalysis B Environ*., **240**, 92-101. https://doi.org/10.1016/j.apcatb.2018.08.077
Zhang, Y., Choi, J.R. and Park, S.J. (2017a), "Thermal conductivity and thermo-physical properties of nanodiamond-attached exfoliated hexagonal boron nitride/epoxy nanocomposites for microelectronics", *Compos. Part A Appl. Sci. Manufact*., **101**, 227-236. https://doi.org/10.1016/j.compositesa.2017.06.019
Zhang, Y., Heo, Y.J., Son, Y.R. and Park, S.J. (2019), "Recent advanced thermal interfacial materials: A review of conducting mechanisms and parameters of carbon materials", *Carbon*, **142**, 445-460. https://doi.org/10.1016/j.carbon.2018.10.077
Zhang, Y., Rhee, K.Y. and Park, S.J. (2017b), "Nanodiamond nanocluster-decorated graphene oxide/epoxy nanocomposites with enhanced mechanical behavior and thermal stability", *Compos. Part B Eng*., **114**, 111-120. https://doi.org/10.1016/j.compositesb.2017.01.051

CC

Appendix A

$$
\begin{aligned}
&\left\{D_{1,i}, D^{\alpha}_{1,i}, D^{\beta}_{1,i}\right\} = \int_{-\frac{h_c}{2}-h_b}^{\frac{h_c}{2}+h_t} Q_{11}(z)*z^i\left\{1,\alpha_{11}(z)\right\}dz, \left\{D_{2,i}, D^{\alpha}_{4,i}, D^{\beta}_{4,i}\right\} = \int_{-\frac{h_c}{2}-h_b}^{\frac{h_c}{2}+h_t} Q_{22}(z)*z^i\left\{1,\alpha_{22}(z)\right\}dz \\
&\left\{D_{3,i}, D^{\alpha}_{2,i}, D^{\beta}_{2,i} D^{\alpha}_{3,i}, D^{\beta}_{3,i}\right\} = \int_{-\frac{h_c}{2}-h_b}^{\frac{h_c}{2}+h_t} Q_{12}(z)*z^i\left\{1,\alpha_{11}(z),\alpha_{22}(z)\right\}dz \\
&\left\{D_{4,i}\right\} = \int_{-\frac{h_c}{2}-h_b}^{\frac{h_c}{2}+h_t} Q_{44}(z)*z^i dz, \left\{D_{5,i}\right\} = \int_{-\frac{h_c}{2}-h_b}^{\frac{h_c}{2}+h_t} Q_{55}(z)*z^i dz \\
&(N_{1,\varphi_0}, N_{2,\varphi_0}) = \int \frac{2\varphi_0}{h_p}(e_{31}, e_{32})dz, (N_{1,\psi_0}, N_{2,\psi_0}) = \int \frac{2\psi_0}{h_p}(q_{31}, q_{32})dz \\
&(N_{1,\varphi}, N_{2,\varphi}) = \int \frac{\pi}{h_p}\sin(\frac{\pi\tilde{z}}{h_p})(e_{31}, e_{32})dz, (N_{1,\psi}, N_{2,\psi}) = \int \frac{\pi}{h_p}\sin(\frac{\pi\tilde{z}}{h_p})(q_{31}, q_{32})dz \\
&(N_{4,\varphi}, N_{5,\varphi}) = \int \cos(\frac{\pi\tilde{z}}{h_p})(e_{15}, \frac{1}{R}e_{24})dz, (N_{4,\psi}, N_{5,\psi}) = \int \cos(\frac{\pi\tilde{z}}{h_p})(q_{15}, \frac{1}{R}q_{24})d \\
&N_{1,D} = \int \cos^2(\frac{\pi\tilde{z}}{h_p})\eta_{11}dz, N_{2,B} = \int \frac{1}{R^2}\cos^2(\frac{\pi\tilde{z}}{h_p})\eta_{22}dz, N_{3,D} = \int \eta_{33}(\frac{\pi}{h_p}\sin(\frac{\pi\tilde{z}}{h_p}))^2 dz \\
&N_{1,B} = \int \cos^2(\frac{\pi\tilde{z}}{h_p})(d_{11}, \frac{1}{R^2}d_{22})dz, N_{2,D} = \int \frac{1}{R^2}\cos^2(\frac{\pi\tilde{z}}{h_p})d_{22}dz, N_{3,B} = \int d_{33}(\frac{\pi}{h_p}\sin(\frac{\pi\tilde{z}}{h_p}))^2 dz \\
&N_{3,B1} = \int d_{33}(\frac{2}{h_p})^2\sin(\frac{\pi\tilde{z}}{h_p})dz, N_{3,D1} = \int \eta_{33}(\frac{2}{h_p})^2\sin(\frac{\pi\tilde{z}}{h_p})dz, (N_{1,B1}, N_{2,B1}) = \int (\mu_{11}, \frac{1}{R^2}\mu_{22})\cos^2(\frac{\pi\tilde{z}}{h_p})dz \\
&N_{3,B2} = \int \mu_{33}(\frac{\pi}{h_p}\sin(\frac{\pi\tilde{z}}{h_p}))^2 dz, N_{3,D2} = \int \mu_{33}(\frac{\pi}{h_p})^2\sin(\frac{\pi\tilde{z}}{h_p})d \\
&(M_{1,\varphi}, M_{2,\varphi}) = \int \frac{\pi z}{h_p}\sin(\frac{\pi\tilde{z}}{h_p})(e_{31}, e_{32})dz, (M_{1,\psi}, M_{2,\psi}) = \int \frac{\pi z}{h_p}\sin(\frac{\pi\tilde{z}}{h_p})(q_{31}, q_{32})dz
\end{aligned}
\tag{A.1}
$$